Epigenetic signatures of regional tau pathology and cognition in the aging and pathological brain.

Short Title: Epigenetic signatures of AD and PART

David Goldberg[1,X], Anil R. Wadhwani[2,X], Nadia Dehghani[2], Lasya P. Sreepada[2,3], Hongxiang Fu[1], Philip L. De Jager[4], David A. Bennett[5], David A. Wolk[2], Edward B. Lee[6], PART Working Group, Kurt Farrell[7], John F. Crary[7], Wanding Zhou[1,6*], Corey T. McMillan[2*]

[1] Center for Computational Genomic Medicine, Children's Hospital of Philadelphia, Philadelphia, PA, USA

[2] Department of Neurology, University of Pennsylvania Perelman School of Medicine, Philadelphia, PA, USA

[3] Department of Bioengineering, School of Engineering and Applied Sciences, University of Pennsylvania, Philadelphia, PA

[4] Department of Neurology, Columbia University Irving Medical Center, New York, NY, USA

[5] Department of Neurological Sciences, Rush University, Chicago, IL, USA

[6] Department of Pathology & Laboratory Medicine, University of Pennsylvania Perelman School of Medicine, Philadelphia, PA, USA

[7] Department of Pathology, Molecular and Cell Based Medicine, Icahn School of Medicine at Mount Sinai, New York, NY, USA

[X] Equal Contribution

*Co-Corresponding Authors

Corey T. McMillan

Penn Frontotemporal Degeneration Center

3700 Hamilton Walk, Richards 606B

Philadelphia, PA. 19104

(e) mcmillac@pennmedicine.upenn.edu (p) 215 614 0987

&

Wanding Zhou

Center for Computational & Genomic Medicine

Children's Hospital of Philadelphia

3501 Civic Center Blvd

Philadelphia, PA, 19104

(e) wanding.zhou@pennmedicine.upenn.edu (p) 215 5900473

Keywords: epigenetics, aging, tau, Alzheimer's disease, primary age-related tauopathy, DNA methylation

ABSTRACT

Primary age-related tauopathy (PART) and Alzheimer's disease (AD) share hippocampal phospho-tau (p-tau) pathology but differ in p-tau extent and amyloid presence. As a result, PART uniquely enables investigation of amyloid-independent p-tau mechanisms during brain aging. We conducted the first epigenome-wide association (EWAS) study of PART, which yielded 13 new and robust p-tau/methylation associations. We then jointly analyzed PART and AD epigenomes to develop "TauAge", novel epigenetic clocks that predict p-tau severity in region-specific, age-, and amyloid-independent manners. Integrative transcriptomic analyses revealed that genes involved in synaptic transmission are related to hippocampal p-tau severity in both PART and AD, while neuroinflammatory genes are related to frontal cortex p-tau severity in AD only. Further, a machine learning classifier based on PART-vs-AD epigenetic differences discriminates neuropathological diagnoses and stratifies indeterminate cases into subgroups with disparity in cognitive impairment. Together, these findings demonstrate the brain epigenome's substantial role in linking tau pathology to cognitive outcomes in aging and AD.

Neurofibrillary tangles (NFTs) consisting of hyperphosphorylated tau (p-tau) are a ubiquitous feature of aging present in nearly every human brain older than 50 years of age[1-5]. However, the spatial distribution and within-region severity of p-tau, as well as the associated degree of cognitive impairment, vary widely across individuals, even after accounting for age and co-pathology[6,7]. In Alzheimer's disease (AD), p-tau originates in a temporo-limbic distribution before spreading to neocortex in concert with the diffuse deposition of amyloid-associated neuritic plaques[2,8]. However, primary age-related tauopathy (PART) represents a distinct aging condition in which p-tau aggregation remains relatively confined to temporo-limbic distribution in the absence of amyloid plaques[6,9-13]. P-tau is molecularly similar in PART and AD and involves hippocampal CA1 and CA3 subfields at early stages[6]. Moreover, genetic studies have revealed a partial overlap of Braak NFT stage in PART and risk for AD[14]. However, PART is unlike AD in that p-tau only rarely spreads to midfrontal or more distant neocortex, and we previously identified a novel locus in the *JADE1* gene as a unique risk determinant of Braak NFT stage in PART[15]. As a result, PART represents a distinct form of brain aging that carries some degree of resistance to AD pathophysiology while still exhibiting some interindividual variation in p-tau severity despite the absence of amyloid. Given these similarities and differences, PART and AD provide a unique human model for interrogating the mechanisms that contribute to p-tau severity and spread in aging. Knowledge gained from these extremes of spectrum of p-tau spread and amyloid presence, or its absence, can additionally be informative for understanding mechanisms underlying indeterminate cases that fall between AD and PART with both relatively sparse plaque burden and limbic-predominant p-tau[12,16,17].

Aging is the strongest risk factor for p-tau. The epigenome provides an important window into modifiers of the PART-vs-AD spectrum and the indeterminate cases between them given that DNA methylation (DNAm) changes widely across the lifespan. While DNAm patterns have been characterized in AD[18-23], prior studies have been limited in several ways. First, blood-derived DNAm epigenetic clocks have linked accelerated epigenetic aging to AD severity[24,25], but the biological basis of these clocks remain obscure and lack brain-specific associations[26]. Second, while studies of cortical brain DNAm have identified CpGs associated with AD neuropathologic change, such as Braak stage NFT distribution[19] and senile plaques[18], they have been performed without regard to within-region severity or the complex interaction of p-tau and amyloid. Therefore, it remains

unclear whether these epigenetic changes are a feature of normal brain aging or if they are a consequence of AD pathophysiology.

Here, we hypothesized that an epigenetic program drives variation in hippocampal p-tau pathology in PART. To understand the epigenetic contributions to p-tau in the aging brain we use several computational approaches to analyze frontal cortex DNAm to disentangle associations between p-tau, amyloid, and aging across the pathological spectrum of PART and AD. This includes the first epigenome-wide association (EWAS) study of PART, the generation of a p-tau clock, "TauAge", that is predictive of age-independent p-tau severity in hippocampus and frontal cortex, and a comparative multivariate classifier of PART and AD that distills the shared biological programs contributing to both conditions from those uniquely protective in PART.

RESULTS

Description of cohorts.

Given that PART differs from AD in that it does not involve amyloid or widespread neocortical dissemination of tau, we generated DNA methylation profiles for 260 individuals in the PART working group (PWG) cohort comprised of autopsy-confirmed definite PART cases (Braak NFT stage I-IV, CERAD = None) and examined hippocampal p-tau by digital histopathology of neurofibrillary p-tau (NFT) density in AT8-stained tissue sections. All PWG samples were interrogated using the Illumina EPIC Human Methylation array for ~850K CpGs (Methods: DNAm data generation). We also performed secondary analyses using public data available from 707 individuals from the Religious Orders Study and Memory and Aging Project (ROSMAP) cohort[18], which includes 176 cases with definite PART (24%; CERAD = None, Braak NFT Stage I-IV) and 157 (22%) cases with definite AD (CERAD = Frequent, Braak NFT Stage V-VI; **Supplemental Table 1**). The ROSMAP cohort includes an additional 365 "Indeterminate" cases with low or intermediate AD neuropathologic change, some of which overlap with a neuropathological diagnosis of probable PART (BRAAK NFT stage I-IV, CERAD = Sparse). All ROSMAP samples were interrogated for DNAm using the Illumina Human Methylation 450 beadchip array and a subset had matched gene expression data generated by the Illumina TruSeq method with modifications as previously described[27]. The unsupervised clustering of DNA methylomes for each cohort was primarily driven by sex and sample plate and did not reveal any patterns relating to hippocampal p-tau load, Braak stage, or CERAD

score (**Extended Data Figure 1A**). Similarly, DNAm-based cellular deconvolution using a reference atlas of neuronal and glial subtypes yielded largely comparable distributions between the PWG and ROSMAP cohorts, with a slight enrichment of superficial cortical layer cell types in the latter (**Extended Data Figure 1B-C)**. Nonetheless, cell-type proportion principal components and individual cell-type proportions did not associate with hippocampal p-tau burden in either cohort (**Extended Data Figure 1D-E**).

An EWAS and novel epigenetic clock, "TauAge", captures hippocampal tau variation in PART.

To identify biological processes that may account for inter-individual variation in hippocampal p-tau pathology, we first performed an epigenome-wide association study (EWAS) in the PWG cohort comprised of 260 PART cases, controlling for age, sex, and sample plate effects**.** We identified thirteen CpG sites that were associated with hippocampal p-tau (FDR < .05), two of which (*cg04905912, cg17649772*) also exceeded the Bonferroni-corrected significance threshold (**Figure 1A)**. Methylations of these CpGs were positively correlated with one another (**Extended Data Figure 2A**), suggesting they may be downstream of a common effector or that they may operate in tandem as part of a concerted epigenetic program. To our knowledge, methylation variation at these 13 loci has not been previously associated with tau pathology in aging or AD across a survey of brain methylation studies[18-23].

Given that DNAm often regulates local gene expression programs[28], we directly evaluated the correlation between each of the 13 significant CpGs with RNA-Seq gene expression of all annotated genes within 10kB of the CpG probe coordinates using matched DNAm:RNA-Seq expression data set from the ROSMAP cohort[27] (Methods: PART Epigenome Wide Association Study, **Figure 1B**). From the 13 CpGs, we identified three significant CpG:gene associations: *cg03815683*:*CDH8*, *cg04522898*:*R3HDM1*, and *cg19212949*:*PEG3*. Downregulation of *CDH8* and *R3HDM1*, but not *PEG3*, further correlated with hippocampal p-tau (**Figure 1B**). One additional pair (cg03595123:*RTN3*) also had a significant association of gene expression with both CpG methylation and hippocampal p-tau but did not survive multiple comparison correction using a false discovery rate (FDR) of 0.05. Thus, p-tau-associated methylation at these newly identified loci correlates with the expression of genes that, in turn, are associated with tau pathology in an independent data set.

CpG methylation can also have *trans*-regulatory effects on gene expression[29]. We therefore expanded our analyses to test the correlation of all genes with methylation of the loci identified in our EWAS (Methods: Differential gene expression analysis) which identified a total of 198 additional genes that were correlated with CpG methylation. Enrichment analysis revealed that these genes were primarily enriched in ontology terms related to ion transport, synaptic transmission, and neuron architecture (**Extended Data Figure 2B**). Most of the significant CpG:gene pairs involved *cg04522898* (**Figure 1C**), suggesting that methylation at this locus may impact large downstream transcriptional networks related to synaptic biology. Together, these findings suggest that p-tau aggregation in the hippocampus is associated with changes in frontal cortical network properties in PART, even in the absence of cortical amyloid deposition.

To further investigate the epigenetic correlates of p-tau pathology independent of amyloid pathology in the PWG cohort, we trained a penalized elastic net (EN) regression model, or "clock", to predict age-adjusted hippocampal p-tau residuals (Methods). The resultant hippocampal clock model, "TauAge", consists of 223 CpGs, including *cg18762422*, one of the CpGs identified by our EWAS. Our model learned the training data with near certainty and closely predicted hippocampal p-tau residuals in testing data (**Figure 1D**). As expected given prior adjustments for age, none of these identified CpGs correlated with chronological age (**Extended Data Figure 2C**). Notably, in contrast to TauAge, existing epigenetic clocks including pan-tissue Horvath[30,31] or brain-specific Cortical[25] clocks were not predictive of age-adjusted residual or unadjusted hippocampal p-tau (**Extended Data Figure 2D**). These results demonstrate that our novel clock of cortical DNAm contains robust signatures indicative of hippocampal p-tau pathological burden in PART, which are separate from known age-related epimutational processes [32].

Distinct TauAge clocks capture p-tau variation in AD cortex and hippocampus

Given the precise predictions using this approach, we next sought to determine if we could accurately calculate TauAge in cases from the ROSMAP cohort, which enriches for the other extreme of the p-tau spectrum, one that is also afflicted by amyloid pathology. In AD, NFTs develop earliest in the entorhinal cortex and hippocampus before spreading to the frontal cortex.[8] As a result, NFT burden in the hippocampus and midfrontal cortex are separate but related measures of p-tau severity that vary between individuals. We leveraged the ROSMAP cohort[18], which exhibits a full spectrum of p-tau and amyloid pathologies ranging from PART to AD, to

train TauAge models for each region. As before, frontal cortical DNA methylomes were used to predict p-tau burden in hippocampus and midfrontal cortex in ROSMAP after adjusting for age. We observed highly accurate predictions for hippocampal TauAge (model size: 461 CpGs) and midfrontal TauAge (model size: 467 CpGs) (**Figure 2A**), while cortical and Horvath epigenetic clocks lacked predictive accuracy (**Extended Data Figure 3A**). Neither TauAge model was enriched in aging-associated CpGs within the ROSMAP cohort (**Extended Data Figure 3B**).

We observed only 8 overlapping CpGs between the hippocampus and midfrontal TauAge models. Indeed, while these TauAge models are moderately correlated (**Extended Data Figure 3C**), hippocampal TauAge is less accurate at predicting midfrontal p-tau burden and similarly midfrontal TauAge is less accurate at predicting hippocampus p-tau burden (**Figure 2B**). This suggests that there are distinct epigenetic traits in cortex that account for regional variation in p-tau burden within an individual. Thus, TauAge does not measure a global property of the brain but rather reflects separate biologies that contribute to similar pathology in different brain regions.

To account for amyloid-dependent processes that may exacerbate p-tau pathology or confound p-tau-specific epigenetic signatures, we re-trained hippocampus and midfrontal TauAge models that, in addition to age, also adjust for total neuritic plaque load (Methods: TauAge model development). The amyloid-adjusted models are additionally accurate and predicting p-tau burden in respective regions (**Extended Data Figure 3D)**, have comparable performance to models that adjust for age alone, and have substantial overlap in constituent feature CpGs in a region-specific fashion (**Figure 2C, Supplemental Table 2**). Taken together, this suggests that TauAge CpGs represent an amyloid-independent and regionally-specific epigenetic program.

Hippocampal TauAge relates to synaptic signaling in PART and AD, whereas midfrontal TauAge relates to inflammation in AD only.

To elucidate the separate underlying biology contributing to each of the PWG and the hippocampus and midfrontal ROSMAP TauAge models, we again leveraged paired DNAm:RNA-Seq data from ROSMAP to identify CpG:Gene pairs with each model (Methods). The gene set correlated with hippocampal TauAge were largely distinct from the midfrontal gene set, mirroring the regional CpG features selected (**Figure 2D**, **Extended Data**

Figure 3E, and Supplemental Table 3). Strikingly, despite differences in histopathological and DNAm techniques, a highly overlapping gene profile emerged for the hippocampal TauAge models trained separately on PART cases from the PWG cohort, PART cases from the ROSMAP cohort, or all cases from the ROSMAP cohort. The gene ontological profile related to all hippocampal TauAge models was enriched for terms related to synaptic transmission, axon biology, and oxidative phosphorylation (**Figure 2E**). Therefore, hippocampal p-tau accumulation in AD and PART appears to be driven by similar epigenetic and genetic features.

In contrast, consistent with spread of p-tau to frontal cortex that occurs uniquely in AD, the CpG:Gene correlations for midfrontal TauAge revealed genes enriched in inflammatory signaling and cytokine production. After corrections for multiple comparisons, we identified that hippocampal TauAge is most strongly related to the altered expression of two genes related to synaptic transmission, and midfrontal TauAge is most strongly related to the upregulation of five genes related to inflammation (**Extended Data Figure 3F)**. Interestingly, one gene, *kinesin family member 5B* **(***KIF5B)*, was common to both midfrontal and hippocampal analyses. Together, these data suggest that hippocampal p-tau severity is associated with altered cortical synaptic activity and connectivity in an amyloid-independent manner both in PART and in AD, while midfrontal p-tau severity may be precipitated by increased inflammation in the cortex in AD only.

Frontal cortex methylations distinguish PART from early AD.

Our EWAS and TauAge models suggest a common epigenomic program related to synaptic transmission contributing to p-tau burden in hippocampus of AD and PART, independent of amyloid, and a disparate epigenomic program in AD related to inflammation. Thus, these observations do not resolve the controversy regarding whether PART simply represents an early pathological prodrome of AD that would eventually manifest with cortical p-tau and amyloid[33] or whether PART represents a distinct neuropathological entity[6]. In an effort to address this, we next evaluated whether an epigenetic classification model could be trained to discern subtle PART or AD propensities. To accomplish this, we first compared TauAge in cases at the extremes of the PART-AD neuropathological spectrum. Additionally, we evaluated the remaining “Indeterminate” cases that fall ambiguously between probable PART and low/intermediate ADNC (CERAD = Sparse, and Braak NFT Stage 0-VI; or CERAD = Moderate-Frequent, and Braak NFT Stage 0-IV). Cases with “No Pathology” (CERAD = “None”,

Braak NFT Stage = 0) were excluded due to their limited number (N = 9), which coincidently further highlights the pervasiveness of p-tau pathology in aging adults.

As expected, given the pervasive involvement of hippocampus in both diseases, hippocampal TauAge was greater in AD compared to both PART and Indeterminate cases (**Extended Data Figure 4A**) and was not distinguishable between PART and Indeterminate cases. In contrast, midfrontal TauAge showed a progressive increase along the PART-AD continuum, suggesting a direct relationship between inflammation and AD neuropathologic change. Despite significant mean differences, the pathology groups had substantial overlap in TauAge which limited our ability to discriminate pathology using these methylation models alone.

We hypothesized that Indeterminate cases may reflect a heterogeneous group in which a subset of cases are epigenetically more similar to PART while others may be more similar to AD. To investigate this possibility, we developed a classifier (PART-AD classifier) to directly stratify Indeterminate cases as Predicted-PART or Predicted-AD from frontal cortical DNAm (**Figure 3A**). To identify CpG features that best distinguish PART from AD, we first performed an EWAS comparing PART to AD individuals with age and sex as covariates and excluded indeterminate cases. Using an FDR of 0.05, we identified 1,214 differentially methylated CpGs between PART and AD (**Extended Data Figure 4B**). Of these, 37 CpGs meet the more stringent experiment-wide level of significance. Only one of these probes (*cg02683408*) has not been previously identified in an AD-related EWAS and emphasizes the similarity of PART with normal aging.

Using only DNAm at these 1,214 CpGs from 100 PART and 89 AD cases, we trained a support vector machine to classify cases as Predicted-PART or Predicted AD. As expected, the resultant PART-AD classifier predicts the pathology of the remaining PART and AD cases from the ROSMAP cohort with 93% sensitivity and 89% specificity (**Figure 3B**). To further validate the classifier, we applied it to cortical DNAm data from 142 individuals defined as Controls (Braak NFT Stage 0-II) or Late Stage AD (Braak NFT Stage V/VI) in an external cohort maintained by the Mt. Sinai Brain Bank (**Extended Data Figure 4C-D**). As expected, the majority of Control cases were classified as Predicted-PART, and the majority of Late Stage AD cases were classified as Predicted-AD, thus validating the classifier's performance and the reproducibility of its underlying epigenetic AD signature.

We then applied the PART-AD classifier to stratify indeterminate cases from the ROSMAP cohort as Predicted-AD or Predicted-PART. Predicted-AD and Predicted-PART cases could not be distinguished clearly from each other directly by their p-tau burden (**Extended Data Figure 4E**), though Predicted-AD cases exhibited modestly more neuritic plaques than Predicted-PART cases on average. Moreover, our TauAge models could not resolve Predicted-AD and Predicted-PART cases (**Figure 3C**), suggesting that the PART-AD classifier measures a tau-independent epigenetic signature.

To further interrogate this additional epigenetic signature, we identified differential methylation at 956 of the 1,214 classifier feature CpGs (**Figure 3D, Supplemental Table 4**) in Indeterminate cases that were classified as Predicted-AD or Predicted-PART. The effect sizes observed were highly concordant with the effect sizes of methylation on diagnosis in PART-AD EWAS conducted during the classifier development (**Extended Data Figure 3F**). Thus, cases of indeterminate pathologic change that do not yet differ substantially in their p-tau burden may have different epigenomes resembling either PART or AD. This distinguishing DNAm signature may relate to different degrees of amyloid burden or different susceptibility to amyloid-associated changes on p-tau.

Further, we directly compared gene expression of the Predicted-PART and the Predicted-AD cases (Methods). 5,895 genes were differentially expressed (**Extended Data Figure 5A, Supplemental Table 5**), and the expression of 81.7% of these genes was also associated with methylation at a feature CpG of the PART-AD classifier (not shown). PART and AD cases and had concordant effect sizes (**Extended Data Figure 5B**). Genes downregulated in Predicted-AD compared to Predicted-PART were highly enriched in oxidative phosphorylation and cellular respiration (**Extended Data Figure 5C**). This may suggest that the cortical spread of tau pathology is preceded by, or may require, cellular metabolic dysfunction. Moreover, genes downregulated in Predicted-PART compared to Predicted-AD were enriched in processes of differentiation and migration (**Extended Data Figure 5D**). This may reflect the decreased abundance of infiltrating immune cells or decreased migration of resident CNS immune cells in PART compared to AD. In summary, the PART-AD classifier uses cortical methylation to resolve Indeterminate cases into higher-risk/AD-like and lower-risk/PART-like subgroups with distinct transcriptomic profiles.

Methylation models complement in predicting cognitive impairment.

Tau pathology is tightly correlated with both age-related and AD-related cognitive impairment[4,34-37]. We, therefore, assessed whether methylation signatures measured by TauAge and the PART-AD classifier were related to cognitive impairment in the ROSMAP cohort, measured by mini-mental status examination ante-mortem a median of 1.14 (interquartile range: 0.56 - 4.25) years from brain donation. Both hippocampal and midfrontal TauAge were inversely correlated with performance on the MMSE (**Figure 4A**). Interestingly, hippocampal TauAge could distinguish individuals with mild cognitive impairment (MCI; MMSE 21-23) from those with no cognitive impairment (MMSE ≥ 24) but not from those with dementia-level impairment (MMSE ≤ 20), whereas a prior epigenetic clock could not[24]. On the other hand, midfrontal TauAge differentiated MCI from demented individuals, but not from those who have a lesser degree of cognitive impairment. Together, the two TauAge models can separate individuals along the spectrum of cognitive impairment, likely reflecting their close association with underlying regional p-tau severity.

Despite similarities in p-tau burden in predicted groups identified by the PART-AD classifier, Predicted-PART individuals scored higher on the MMSE than Predicted-AD individuals (**Figure 4B**). Interestingly, the effect of hippocampal TauAge on MMSE is more pronounced in the Predicted-AD individuals than in Predicted-PART individuals (**Figure 4C**). Therefore, while PART and AD share similar hippocampal p-tau, susceptibility to metabolic dysfunction and immune cell infiltration may result in more dramatic cognitive impairment in AD. As a corollary, PART resistance to metabolic dysfunction and lack of inflammation may mediate more resilient cognitive aging.

Finally, to quantify the relative contributions of the TauAge and the PART-AD classifier signatures in predicting cognitive resilience, we constructed several multiple regression models and evaluated the variance explained in MMSE (**Figure 4D**). While age alone explained only about 2% of the overall variance in MMSE performance, adding the methylation-based models above increased the adjusted R-squared to 32%. Hippocampal TauAge, midfrontal TauAge, and the PART classifier additively improved the summative model's performance, suggesting that each may measure a distinct aspect of pathophysiology that contributes to cognitive impairment in aging and AD.

DISCUSSION

This study provides the first characterization of the epigenetic landscape of PART. By carefully disentangling correlations between p-tau, amyloid, and DNAm, across a neuropathological spectrum of PART and AD we define for the first time an amyloid-independent epigenetic clock linked with regional p-tau pathology. Two key processes – synaptic signaling and neuroinflammation – differentially associate with early hippocampal p-tau and its later spread to the frontal cortex, respectively. Critically, these findings highlight important molecular insights into age- and AD-associated tau biology that we discuss below in detail.

TauAge is a novel methylation-based measure of within-region p-tau severity.

To differ from generalized measures of epigenetic age, we rationalized that we could determine a more precise and relevant set of CpGs biologically relevant to a specific age-related pathology by regressing DNAm directly onto the target variable. We, therefore, developed TauAge, a novel bioinformatic strategy to identify a robust pattern of DNAm associated with p-tau variation. Indeed, TauAge predicted hippocampal p-tau variation in PART from cortical DNA from aged individuals in our new cohort, whereas two previously developed epigenetic clocks, one tissue-type independent and one cortex-specific, failed to model both hippocampal p-tau burden and variation. We were able to replicate our approach in a second cohort, both in the subset of individuals with PART and in the entire cohort exhibiting the full spectrum of AD neuropathologic change. Given these findings, TauAge may be a useful tool to apply to interrogate additional datasets and to further probe the underlying biology of tau aggregation and spread.

TauAge has several key properties that distinguish it from more nonspecific measures of epigenetic aging. First, by modeling an age-adjusted residual of p-tau burden, TauAge reflects brain-specific biological processes that are age-independent. Indeed, no TauAge model was enriched for known age-associated CpGs, and therefore, the feature CpGs are more likely key mediators in the pathophysiology of tauopathies at every stage of life.

Second, previous studies have largely related DNAm with Braak NFT stage, a measure of the anatomic distribution of p-tau and severity of global cognitive impairment. In contrast, TauAge measures the within-region severity in p-tau burden which is more closely related to a specific cognitive symptom, such as memory

difficulties. One prior report has linked two measures of epigenetic age acceleration to presence of dementia but failed to separate individuals with no or mild cognitive impairment.[24] TauAge, however, is continuously correlated with mini-mental status examination, and hippocampal TauAge is the first epigenetic measure that can distinguish MCI from cognitively unimpaired individuals.

Third, TauAge has the property that its region specific. Unlike other epigenetic models which lump different pathologies, attributing them to a single age-related biological process, our TauAge method yielded different feature CpGs related to hippocampal and midfrontal p-tau burden. Critically, this is the first demonstration that subsets of cortical DNAm can differ with regards to local and remote pathology, and that both can be measured simultaneously. All hippocampal TauAge models demonstrated substantial overlap in associated differential gene expression and gene ontological profiles, suggesting that technical differences in DNAm platforms or histopathological strategies may account for differences in the strongest-associated feature CpGs in each model. Additional studies that similarly combine DNAm with careful quantitative histopathology are needed to evaluate the generalizability of the TauAge approach, and such studies have the potential to better elucidate region specific age- or pathology-related brain changes.

Lastly, TauAge is modifiable by features beyond age. Because of the complex and synergistic interactions between amyloid and p-tau, we calculated an amyloid-adjusted TauAge which similarly predicted regional p-tau burden. Interrogating the similarities between the unadjusted and amyloid-adjusted models allowed us to filter for CpGs that are more likely to be amyloid-independent modifiers of tau pathophysiology. In light of this innovative approach, we focused on these amyloid-independent CpGs in subsequent analyses.

Hippocampal and midfrontal tau implicate distinct epigenetic programs.

PART and AD both exhibit p-tau neuropathology in the hippocampus, and our evidence suggests that the epigenetic and transcriptomic features related to hippocampal p-tau are similar in both neuropathological conditions. However, a key difference between PART and AD is the relative sparing of p-tau inclusions in the frontal cortex for PART. Midfrontal TauAge could distinguish individuals with dementia from those with mild cognitive impairment, likely leveraging an AD-specific epigenetic signature related to a T-cell and macrophage-mediated axis of inflammation.

We identified an additional epigenetic signature that was unique to AD and was detected by the PART-AD classifier, which was trained on differential methylation from cases at the extremes of the PART-AD neuropathological spectrum. The classifier was agnostic to neuropathological traits yet its performance was highly accurate in classifying independent cases within the ROSMAP and Mt Sinai Brain Bank (MSBB) cohorts[38].

Critically, our evidence of an inflammatory pathway relating to AD midfrontal p-tau and our classifier observation of distinct epigenetic profiles in PART and AD add to the growing evidence that these neuropathological conditions may have distinct molecular bases. Based on the current findings and our prior genetic studies[14,15], we posit that PART may reflect a model of resistance to p-tau spread that is moderated through both epigenetic and genetic factors.

DNAm can be associated with hippocampal tau pathology in aging independently of amyloid.

In support of the hypothesis that PART is a non-AD biological processes that affects hippocampal p-tau, we used a traditional EWAS approach to identify 13 novel CpG sites that have not previously been implicated in brain aging, AD, or other tauopathies. Through an integrative analysis of DNAm with bulk transcriptomics, we further characterized three candidate genes (*CDH8*, *R3HDM1*, and *PEG3*) as potential *cis* mediators of tau-associated differential DNAm. Each of these genes has previously been associated altered neuronal connectivity.[39-42] Of note, the *R3HDM1* gene has been linked with age with DNAm at *cg04522898* in whole blood and an increase in *R3HDM1* expression in pediatric populations.[43] Further studies are required to validate the association of DNAm with gene expression from these adjacent loci or hippocampal p-tau burden.

While *R3HDM1* has not been well-characterized its locus harbors the *pri-miR-128-1* gene[44], and miR-128 has been implicated in synaptic plasticity and cellular survival by additional epigenetic mechanisms.[45-47] Indeed, when we expanded our study to assess for additional CpG-gene expression relationships, we found 198 genes that were differentially expressed in relation to differential methylation of at least one of the 13 CpG sites. A majority of these transgene expression effects, including on *MAPT*, were related to methylation at *cg04522898* which lies within the *R3HDM1* locus and may relate to miR-128 function. While functional validation is required to directly investigate the potential mechanistic role of these genes in tau biology, this study points to several novel genomic loci that may contribute mechanistically to p-tau aggregation in hippocampus.

Synaptic signaling is a shared determinant of hippocampal p-tau burden in both PART and AD.

Age is the greatest risk factor for PART and AD. Numerous age-related biological changes, such as telomere shortening, genomic instability, mitochondrial dysfunction, loss of proteostasis, and epigenetic changes, have been implicated in AD pathology[48]. In this study, we demonstrate that variation in gene expression related to synaptic transmission and plasticity associates strongly with severity of hippocampal tau pathology. Our data suggest that an age-related epigenetic program related to synaptic transmission and plasticity drives hippocampal tau pathology in both PART and AD. Notably, this occurs in the absence of amyloid.

Synapse dysfunction is a key early hallmark of AD[49,50]. Similarly, synaptic dysregulation may occur in aging and in PART, though there is less consensus on specific molecular etiologies[51-55]. We observed that greater age-related hippocampal p-tau burden is associated largely with the downregulation of synaptic transcripts such as *neuroligin 4 Y-linked (NLGN4Y)*, a poorly studied gene believed to interact with neurexins and be essential for synapse formation[56-58]. Interestingly, we also find that increased expression of *kinesin family member 5B* **(***KIF5B)*, a microtubule motor associated with lysosomal function and mitochondrial localization, positively correlates with hippocampal and midfrontal p-tau[59,60]. Strikingly, this finding from our human tissue study independently validates a similar observation in the P301S murine model of tauopathy[61]. Therefore, abnormal cytoskeletal trafficking may link with the transcriptomic signature for dysregulated oxidative phosphorylation detected by our multiple methylation models and may synergistically connect to abnormal tau pathology.

Our findings independently corroborate but are unique from prior transcriptomic studies in AD brain, which have similarly implicated synaptic dysregulation in AD[62-65]. We first identify DNAm differences associated with hippocampal p-tau and then relate differential methylation to differential gene expression. Moreover, in our study, we focused on the subset of CpGs and associated genes that are likely to be amyloid-independent p-tau modifiers. Lastly, ours is the only study to specifically analyze individuals with PART, and we find that differential methylation converged on overlapping synapse-related genes in both the PWG and ROSMAP cohorts.

We initially computed age-expected values for hippocampal tau pathology for PART cases alone to minimize any confounding effect of pathology-associated DNAm in the model. To our surprise, there was not significant overlap in the CpG features of EN models trained separately on PART cases from either the PWG or ROSMAP cohort. Nonetheless, while unable to directly cross-validate methylation models across cohorts, there was

substantial intersection of the differentially expressed genes regulated by the respective feature CpGs of the two models. There are also several notable methodological differences across PWG and ROSMAP cohorts that may account for observed differences between them. First, the two studies ascertain DNAm using two similar but distinct array chips, which include nonoverlapping sets of CpG sites. Therefore, a model trained on one cohort DNAm may not be directly applied to another dataset unless unique CpGs are excluded, in turn reducing the depth of genomic coverage and biological insight. Second, the two studies using different immunohistochemistry methods that vary in their sensitivity to p-tau affinity. Specifically, in ROSMAP, NFTs were identified by silver stain, which is more sensitive to mature NFTs, whereas in PWG, NFTs were identified by AT8 antibody, which detects both mature and immature p-tau assemblies. Despite these technical differences at the level microarray and histopathology, the convergence of the models at the gene expression level suggests that they are two convergent views of the same underlying biology.

Importantly, DNAm and gene expression data are obtained in the frontal cortex, remotely from the site of hippocampal pathology. A limitation of our study the casual relationship between of cortical DNAm and neuropathology cannot be ascertained directly. DNAm may change due to hippocampal interruption of cortical afferent input or via direct molecular effects of p-tau that spreads in an anterograde trans-synaptic fashion from the hippocampus to the cortex. Indeed, cortical DNAm changes may mirror similar changes that occur within the hippocampus during the earliest phases of or even prior to p-tau aggregation. These possibilities may be resolved in subsequent studies through the use of animal tau seeding models and by concomitant measurement of DNAm and gene expression in both brain regions.

PART represents a cognitively resilient form of aging.

Our machine learning-based analyses of DNA methylation suggest that AD and PART both involve dysregulation of synaptic transmission and plasticity, raising the possibility that PART can set the stage for the development of AD. Individuals with lower p-tau burden than expected for their age exhibit an epigenetic signature indicative of preserved synaptic function, which may confer protection at the onset of amyloid aggregation. In other words, we suspect that a component of the age-associated AD risk is due to underlying

PART. Further research is required to determine whether amyloid-independent brain DNA methylation differences consistently predict susceptibility to hippocampal tau pathology in additional datasets.

Importantly, our PART-AD classifier uses an epigenetic signature distinct from the TauAge models to stratify cases with indeterminate pathology. Gene ontology analysis identified a role for increased metabolic capacity in Predicted PART cases and increased cell migration and transcription in Predicted AD. Given numerous other reports of inflammation-associated transcriptomic changes in brain[66-70], The latter may represent an effect of infiltrating inflammatory cells, and this can be evaluated in more detailed studies using single-cell RNA sequencing or spatial transcriptomics.

There was a weak association with neuritic plaque burden, but p-tau burden was similar in both predicted PART and predicted AD cases. Strikingly, those predicted as PART exhibited uniformly better cognitive performance. Within predicted PART cases there still was an appreciable decline in cognitive performance associated with higher TauAge; however this effect was far more pronounced in predicted AD cases. This suggests a potential additive effect of synaptic dysregulation and inflammation on cognition in AD.

Importantly, our three novel methylation models relate to distinct underlying biology and synergistically measure cognitive impairment, as evidenced by the increased performance of a summative model of MMSE that includes all three models. Hippocampal TauAge can distinguish MCI from the cognitively unimpaired, and it appears to model synaptic pathophysiology shared by PART and AD. Together, these findings lend credence to the hypothesis that age-associated cognitive impairment due to hippocampal dysfunction may precede and be requisite for typical AD.

From here, despite similarities in pathological burden, individuals with early AD begin to diverge from PART in a manner detectable by our PART-AD classifier and related to an epigenetic signature of decreased brain metabolic failure. Finally, as p-tau disseminates widely through the neocortex, mid frontal TauAge increases, distinguishing MCI from dementia-level of impairment and relating to NK- and T-cell-mediated inflammation. This absence of an inflammatory signature in PART cases is very likely neuroprotective and indicates a new pathophysiological axis differentiating PART from AD.

Taken together, these models further clarify the molecular similarities and differences between AD and PART and highlight a role for amyloid-independent interindividual variation in hippocampal p-tau severity as a separate modifiable risk factor for AD and age-associated cognitive changes more broadly.

LEGENDS

Figure 1: Hippocampal p-tau burden in PART associates with a DNAm signature related to synaptic signaling and cytoskeletal architecture.

(A) Epigenome-wide association study (EWAS) of hippocampal p-tau, covarying for age, sex, and batch, reveals 13 novel CpGs (red). Dashed line indicates level of significance after correction for multiple comparisons: False Discovery Rate (FDR) < 0.05 (Black) and Bonferroni-adjusted p-value < 0.05 (Blue).

(B) Table of EWAS CpGs and adjacent genes, along with effect size of hippocampal p-tau burden on CpG methylation (blue outline) in PWG cohort, Pearson correlation coefficients of CpG methylation and gene expression (green outline) in ROSMAP cohort, and effect size of hippocampal p-tau burden on gene expression (red outline) in ROSMAP cohort. Not all CpG:gene pairs could be tested in both cohorts due to lack of detectable RNA expression or absence of a CpG probe on the Human Methylation450 (HM450) beadchip array. n = number of cases. kb = kilobase.

(C) Compared to other EWAS CpGs, methylation at *cg04522898* correlates with the expression of a large network of genes related to synaptic transmission, neuron projection, and ion transport. Red edges = positive correlation, blue edges = negative correlation.

(D) TauAge predicts age-adjusted hippocampal p-tau residuals with high accuracy in the PWG cohort. [Training] n = 174, Pearson's Cor = 0.9997 and P < 2.2e-16; [Testing] n = 86, Cor=0.77 and P < 2.2e-16. F = female, M = male.

Figure 2: TauAge predicts p-tau severity in a region-specific manner.

(A) TauAge predicts both hippocampal (left) and midfrontal (right) age-adjusted p-tau residuals with high accuracy in the ROSMAP cohort. For hippocampal TauAge, one outlier is not displayed due to axes limits but was included in statistical testing. [hippocampus, training] n = 416, Pearson Cor = 0.9997 and P = 0; [hippocampus, testing] n = 291, Pearson Cor = 0.66, P = 1.342e-37; [midfrontal, training] n = 416, Cor = 0.9996 and P = 0; [midfrontal, testing] n = 291, Pearson Cor = 0.69 and P = 1.68e-42. F = female, M = male.

(B) In contrast to TauAge, region-discordant models fail to predict p-tau residuals. Models trained to predict hippocampal age-adjusted p-tau residual from midfrontal p-tau EWAS CpGs (left) do not learn or perform as well as the region-concordant hippocampal TauAge model. The same is true for the converse condition (right [hippocampus, training] n = 416, Pearson's Cor = 0.66 and P = 1.19e-54; [hippocampus, testing] n = 291, Pearson's Cor = 0.197 and P = 0.0007; [midfrontal, training] n = 416, Pearson's Cor = 0.64 and P = 8.4e=-49; [midfrontal, testing] n = 291, Pearson's Cor = 0.305 and P = 1.09e-7. F = female, M = male.

(C) Upset plot demonstrating number of disparate and overlapping final feature CpGs in each TauAge model. The overlapping CpGs from the unadjusted and amyloid-adjusted TauAge models are suspected to be amyloid-independent epigenetic modifiers of p-tau in hippocampus (purple) and midfrontal cortex (orange).

(D) Heatmap demonstrates substantial overlap of methylation-associated gene expression in hippocampal TauAge models developed from PART cases in two independent cohorts. This overlap is shared with the amyloid-adjusted hippocampal TauAge model from all cases in the ROSMAP cohort, but distinct from the amyloid-adjusted midfrontal TauAge model genes from the same set of individuals.

(E) The feature CpGs of each hippocampal TauAge model are associated with expression of genes enriched for gene ontology (GO) terms related to synaptic transmission, oxidative phosphorylation, and cytoskeletal architecture. In contrast, the feature CpGs of the midfrontal TauAge model are associated with expression of genes enriched for GO terms related to inflammation. Statistical testing is detailed in Methods.

Figure 3: The PART-AD classifier measures an additional epigenetic signature that distinguishes PART from AD.

(A) Schematic of training and application of the PART-AD classifier. DNAm from cases meeting definition for PART (n=100) or AD (n=89) from the ROSMAP were used to train a support vector machine, which was in turn tested on for accuracy on the remaining ROSMAP and on an external validation cohort (as in Supplemental Figure 4C. The PART-AD classifier was then used to segregate Indeterminate cases (n = 365) from the ROSMAP cohort into Predicted-PART and Predicted-AD cases for subsequent analyses.

(B) Confusion matrix demonstrates highly accurate performance of the PART-AD classifier on test cases from the ROSMAP cohort. Binomial Test n= 105 and P=4.67e-06..

(C) Predicted-AD and Predicted-PART in the ROSMAP cohort cases could not be distinguished by either unadjusted or amyloid-adjusted TauAge models. For hippocampal TauAge, one outlier is not displayed due to axes limits but was included in statistical testing. Pairwise t-tests: n = 366. n.s. = not significant.

(D) Volcano plot of differentially methylated CpGs between Predicted-PART and Predicted-AD cases from the ROSMAP cohort (CpG methylation ~ age + sex + sample_plate + prediction group): n = 366. Highlighted are 956 significant CpGs after correction with an FDR < 0.05 (red line).

Figure 4: TauAge and the PART-AD classifier estimate cognitive impairment better than age or neuropathologic change alone.

(A) Increasing hippocampal (left) and midfrontal (right) TauAge in the ROSMAP cohort are associated with decreasing performance on the mini-mental status examination (MMSE) and, therefore, increasing cognitive impairment. For hippocampal TauAge, one outlier is not displayed due to axes limits but was included in statistical testing. Statistical test was a one-way ANOVA followed by Tukey's range test: n = 707.

(B) Predicted-AD cases exhibit lower MMSE score and, therefore, greater cognitive impairment compared to Predicted-PART cases in the ROSMAP cohort. Statistical test was a two-tailed *t*-test: n = 366.

(C) There is an inverse correlation of hippocampal TauAge and MMSE score. The slope of the effect is greater in Predicted-AD cases compared to Predicted-PART cases. For hippocampal TauAge, one outlier is not displayed due to axes limits but was included in statistical testing. [Predicted-PART] n= 392, Cor = -0.102, and P = 0.045; [Predicted-AD] n= 315, Cor = -0.33, and P = 4.58e-05.

(D) Hippocampal TauAge, midfrontal TauAge, and the PART-AD classifer better correlate with cognitive impairment compared to either age or AD neuropathologic change (ADNC) alone.

Supplemental Table 1: Individual characteristics for the PART Working Group (PWG) and Religious Orders Study and Memory and Aging Project (ROSMAP) cohorts separated by neuropathological case definitions (Methods).

Supplemental Table 2: TauAge feature CpGs.

Supplemental Table 3: TauAge-associated differentially-expressed genes.

Supplemental Table 4: PART-AD classifier feature CpGs.

Supplemental Table 5: PART-associated differentially expressed genes.

Extended Data Figure S1: Methylation structure.

(A) T-distributed stochastic neighbor embedding (t-SNE) clustering of DNAm in both cohorts shows organization of data by sex and sample plate, but not hippocampal p-tau burden, Braak NFT stage, or CERAD score.
(B) Cell type proportion estimates for 20 major brain cell types from methylation-based deconvolution in PWG and ROSMAP.
(C) Principal component analysis of DNAm demonstrates mild differences in cell type composition between two cohorts.
(D) Regressing hippocampal p-tau burden on cell type proportion principal components demonstrates that p-tau is not significantly associated with an individual sample's cell type composition in either cohort.
(E) Regressing hippocampal p-tau on cell type proportions, covarying for age and sex, did not reveal an association for any cell type in PWG cases. FDR = False Discovery Rate

Extended Data Figure 2: Characterization of PART EWAS and Hippocampal TauAge CpGs.

(A) Heatmap demonstrates that EWAS CpGs are correlated with one another (Pearson's correlation).
(B) EWAS CpG methylation is correlated with expression of genes enriched for gene ontology (GO) terms related to synaptic transmission, ion transport, and cytoskeletal architecture. Statistical testing is detailed in Methods.
(C) Volcano plot showing effects sizes of aging on CpG methylation in the PWG cohort. Hippocampal TauAge feature CpGs are age-independent.
(D) Epigenetic age acceleration residuals (horizontal axis) calculated by the Horvath pan-tissue clock or Cortical brain-specific clock do not correlate with the actual hippocampal p-tau burden nor the age-adjusted p-tau residual. Statistical test was Pearson correlation. n = 260.

Extended Data Figure 3: Characterization of ROSMAP hippocampal and midfrontal TauAge CpGs.

(A) Epigenetic age acceleration (horizontal axis) calculated by the Horvath pan-tissue clock (left) and Cortical brain-specific clock (right) do not correlate with hippocampal age-adjusted p-tau in the ROSMAP cohort. Statistical test was Pearson correlation: n = 707 [Horvath], 707 [Cortical].
(B) Volcano plot demonstrating that hippocampal (purple) and midfrontal (orange) TauAge feature CpGs are largely age-independent in the ROSMAP cohort.
(C) Hippocampal and midfrontal TauAge are moderately correlated (Pearson's cor = 0.366, P = 1.3e-10. One outlier is not displayed due to axes limits but was included in statistical testing. n = 291 TauAge testing cases.
(D) Amyloid-adjusted TauAge predicts both hippocampal (left) and midfrontal (right) age- and amyloid-adjusted p-tau residuals with high accuracy in the ROSMAP cohort. [hippocampus, training] n = 416, Pearson Cor = 0.9992 and P = 0; [hippocampus,testing] n = 291, Pearson Cor = 0.75, P = 5.35e-54; [midfrontal, training] n = 416, Cor = 0.9995 and P = 0; [midfrontal, testing] n = 291, Pearson Cor = 0.69 and P = 5.02e-43. F = female, M = male. For hippocampal TauAge, one outlier is not displayed due to axes limits but was included in statistical testing.
(E) Upset plot demonstrating number of overlapping and distinct genes for different TauAge model CpG sets. Genes were identified for correlation with the model CpGs. "Amyloid independent" corresponds to the CpG sets from figure 2C shared between amyloid and non-amyloid adjust models. R = ROSMAP, P = PWG. Figure is truncated to highlight overlap. Complete listing of genes in Supplemental Table 3.
(F) Violin plots illustrating the effect size of regional p-tau severity on gene expression for synaptic transmission genes identified from hippocampal TauAge models (left) and inflammation related genes from TauAge midfrontal models (right). Significant genes (FDR<.05) highlighted. Statistical testing is detailed in Methods.

Extended Data Figure 4: DNAm distinguishes indeterminate cases along the PART-AD continuum.

(A) Hippocampal (left) and midfrontal (right) TauAge increase along the PART-AD continuum. Midfrontal TauAge more strongly distinguishes indeterminate cases from PART. For hippocampal TauAge, one outlier is not displayed due to axes limits but was included in statistical testing. n= 290 TauAge test cases.

(B) EWAS comparing PART and AD cases, covarying for age, sex, and batch, reveals 1,214 differentially methylated CpGs, one of which (red) has not been previously reported in a prior study. Dashed line indicates level of significance after correction for multiple comparisons: False Discovery Rate (FDR) < 0.05 (Black) and Bonferroni-adjusted p-value < 0.05 (Blue).

(C) Schematic of training and testing of the PART-AD classifier. DNAm from ROSMAP cases meeting definition for PART (n=100) or AD (n=89) were used to train a support vector machine, which was tested for accuracy on the remaining PART (n=76) or AD (n=29) cases in the ROSMAP cohort, and on an external validation cohort from the Mt. Sinai Brain Bank (MSBB), where cases are classified as Control (Braak NFT Stage 0-II), or Late Stage AD (Braak NFT Stage V-VI).

(D) Confusion matrix demonstrates accurate performance of the PART-AD classifier on cases from an external validation cohort. Note that in this cohort, cases are predicted as Late Stage AD (Braak NFT stage V-VI) or control (Braak NFT stage 0-II), without regard to amyloid status. Therefore, some cases that meet our definition of PART are present in both groups. Binomial test, P = 1.48e-05, n= 142.

(E) Hippocampal and midfrontal p-tau neurofibrillary tangles (NFTs) were similar between Predicted-PART and Predicted-AD cases, whereas Predicted-AD cases exhibited modestly increased neuritic plaques in both regions. Pairwise t-tests n = 366. n.s. = not significant.

(F) Correlation of differential methylation effect size between PART and AD cases (horizontal axis) and Predicted-PART and Predicted-AD cases (vertical axis) for all significant CpGs in Figure 3D. Effect sizes are largely concordant and mildly attenuated. Pearson's correlation: n = 956.

Extended Data Figure 5: Predicted-PART and Predicted-AD have a distinct transcriptomic signature.

(A) Analysis of ROSMAP RNA-sequencing data reveals 5,895 differentially expressed genes between Predicted-PART and Predicted-AD.. Expression of 4,814 of these genes are also associated with differential-methylation at a feature CpG of the PART-AD classifier.

(B) Correlation of differential gene expression effect size between PART and AD cases (horizontal axis) and Predicted-PART and Predicted-AD cases (vertical axis) for all significant genes in (A) Pearson Cor = 0.935 and P < 2.2e-16.

(C) Genes downregulated in Predicted-AD compared to Predicted-PART are enriched for gene ontology (GO) terms related to oxidative phosphorylation and cellular respiration. Statistical testing is detailed in Methods.

(D) Genes downregulated in Predicted-PART compared to Predicted-AD are enriched for gene ontology (GO) terms related to cell differentiation and migration. Statistical testing is detailed in Methods.

ONLINE METHODS

Patient Selection and Cohorts. Fresh-frozen brain tissue was obtained from the contributing centers in the PART Working Group (PWG) as previously described[15]. All tissue was used in accordance with the relevant guidelines and regulations of the respective institutions. Inclusion criteria were individuals with normal cognition, mild cognitive impairment (any type) and dementia. Cognitive status was determined either premortem or postmortem by a clinical chart review, mini-mental score, or clinical dementia rating[71,72]. Neuropathological assessments were performed at the respective centers using standardized criteria including Consortium to Establish a Registry for Alzheimer's Disease (CERAD) neuritic plaque assessment and Braak neurofibrillary tangle staging.[8,73] In addition, formalin fixed paraffin-embedded tissue sections were obtained and reevaluated by the study investigators to confirm the lack of Aβ and degree of PART tau pathology as previously described[74]. Clinical exclusion criteria were motor neuron disease, parkinsonism, and frontotemporal dementia. Neuropathological exclusion criteria were other degenerative diseases associated with NFTs (i.e., AD, progressive supranuclear palsy [PSP], corticobasal degeneration [CBD], chronic traumatic encephalopathy [CTE], frontotemporal lobar degeneration-tau [FTLD-tau], Pick disease (PiD), Guam amyotrophic lateral sclerosis/parkinsonism–dementia, subacute sclerosing panencephalitis, globular glial tauopathy). Individuals with aging-related tau astrogliopathy (ARTAG) were not excluded[75]. Characteristics and procedures of the Religious Orders Study and Memory and Aging Project (ROSMAP) were as previously described[76]. Characteristics and procedures of the Mount Sinai Brain Bank (MSBB) cohort were as previously described[38].

Case definitions and histopathology. To allow for comparisons between cohorts and to minimize confounding due to overlapping pathologies, we limited our analyses using the following case definitions, using variables common across PWG and ROSMAP cohorts. We conserve our definition of PART to "definite PART" defined as Braak NFT stage I-IV and CERAD = None[6]. For AD, we restrict to cases that meet Braak NFT stage VI-V and CERAD = Frequent[16]. Remaining cases were termed Indeterminate. Digital histopathology in the PWG cohort was performed as previously described[77]. Briefly, stains were performed on 4 μm-thick formalin-fixed paraffin-embedded (FFPE) sections stained with AT8 antibody. Sections from the body of the hippocampus were targeted, but this neuroanatomical landmark was not represented in all sections, and there was some variability noted with regard to representation along the anterior–posterior axis. Whole slice images were scanned using an Aperio CS2 (Leica Biosystems, Wetzlar Germany) digital slide scanner at 20 × magnification, and neurofibrillary tangle density was calculated via a SegNet model architecture as previously detailed[78]. Manual histopathology assessment in the ROSMAP cohort was performed by independent neuropathological assessment of silver-stained tissue, as previously described[79]. To validate the PART-AD classifier, we tested it it on cases from the MSBB cohort, which the investigators previously defined as Control (Braak NFT Stage 0-II), or Late Stage AD (Braak NFT Stave V-VI).

DNAm data generation. In the PWG cohort, DNA was extracted from the frontal cortex. Bisulfite converted DNA was profiled using the Illumina Infinium MethylationEPIC bead chip array at the Center for Applied Genomics core at the Children's Hospital of Philadelphia. In the ROSMAP cohort, DNA extraction and methylation profiling using the Illumina Infinium Human Methylation450 bead chip assay was performed as previously described[18]. Raw data from both cohorts was used and subjected to the same standard manufacture recommended preprocessing and quality control pipeline using the SeSAMe R package (version 1.22.0). Beta values were extracted using the openSesame function with default parameters as previously described[80].

Unsupervised clustering analysis: CpGs with >50% missingness across all samples were removed and remaining missing values were imputed using the beta value mean from non-missing samples. tSNE analysis was performed using the Rtsne package (version 0.16) with a perplexity of 30.

Cell type deconvolution: Beta matrices for PWG and ROSMAP cohorts were filtered for common CpGs with coverage across 75% or more of samples in both cohorts. A reference matrix for 20 major brain cell types was constructed by performing one vs. all non-parametric analyses of pseudobulk methylomes obtained from publicly availably single cell WGBS data[81-83]. Reference-based cellular deconvolution was performed using the EpiDISH R package (version 2.16.0) with the robust partial correlations (RPC) method. Principal component analysis was performed with the prcomp function from the stats package (version 4.4.0) using the cell type proportions as input features.

PART Epigenome Wide Association Study (EWAS): CpG methylation (CpGm) was regressed on logarithmically-transformed hippocampal p-tau (hip_p-tau) with age, sex and sample plate added as covariates. [Model: CpGm ~ age + sex + sample plate + *log*(hip_p-tau + 1)] Modelling was performed using the DML() function from the SeSAMe R package (version 1.22.0). P values for each modelled CpG were corrected for multiple comparisons by the false discovery rate (FDR) method, and only those with FDR < .05 were considered for further analysis. Gene annotations were retrieved using the sesameData_txnToGeneGRanges function from the sesameData package (version 1.21.9) and intersected with EWAS hit CpGs (expanded by 10KB) using the subsetByOverlaps function from the GenomicRanges package (version 1.57.1).

TauAge model development: TauAge is a novel statistical model that uses methylation at a distinct set of feature CpGs to predict an age-adjusted regional p-tau residual. To calculate the age-adjusted p-tau residual, logarithmically-transformed hippocampal or midfrontal p-tau was regressed on age [*log*(p-tau + 1) ~ age]. Amyloid-adjusted TauAge similarly predicts an age- and amyloid-adjusted p-tau residual. To calculate age- and amyloid-adjusted residuals, logarithmically-transformed total brain neuritic plaques were added as a covariate [*log*(p-tau + 1) ~ age + *log*(plaque + 1)]. For each model, training data were balanced to include equal numbers of male and female samples (80% of lesser-represented sex), and remaining samples were used for testing. For any given cohort and region, an elastic net (EN) regression of p-tau residuals on CpGm was performed using the cv.glmnet function from the glmnet package (version 4.1.8) with an alpha parameter of 0.5 and 10-fold cross validation. For each p-tau residual target, CpG features were rank ordered according to the unadjusted P-value from running a univariate EWAS [Model: CpGm ~ age + sex + sample plate + *log*(variable + 1)]. Feature sizes were scanned from the top 2,000- to top 30,000-ranked CpGs, and models with the most highly correlated predictions to actual values on testing data were selected for further analysis. For hippocampal TauAge, there was one outlier in the ROSMAP cohort was 6 standard deviations below the cohort mean. This outlier was excluded from visualization but was included in all statistical analyses. To confirm the within-region specificity of TauAge models in the ROSMAP cohort, separate models were trained to predict one region's p-tau residual using the opposite region's feature CpGs.

Epigenetic age analysis: Missing values from processed beta matrices were imputed using the row mean from non-missing samples, and epigenetic age estimates (mAge) were computed using the methyAge function from the dnaMethyAge package (version 0.2.0)[84]. Age acceleration was computed by calculating the residual of epigenetic age regressed onto the chronological age [mAge ~ Age]. Pearson correlations were computed between the age acceleration residuals and p-tau load or p-tau residual.

PART-AD classifier development: For feature selection, CpG methylation was regressed on pathology group (PART vs. High pathologic change AD) with age, sex and sample plate added as covariates (CpGm ~ age + sex + sample plate + pathology).. PART cases were those with Braak staging I-IV and a Cerad score of 0, while high pathologic change AD were cases with Braak stage III-VI, Cerad 2-3. Modelling was performed using the DML function from the SeSAMe R package (version 1.22.0). P values for modelled CpGs were FDR adjusted and those with FDR < .05 were used as features (1,214 total). For CpGs with missing values, the mean over all other samples was used for imputation. 100 PART and 89 AD cases were used to train a support vector machine classifier using the svm function (kernel="linear") from the e1071 package (version 1.7-14). The model was tested on an additional 29 AD samples and 76 PART samples not seen during the training process. Performance statistics were computed using the Caret library (version 6.0-94)[85].

Differential gene expression analysis: Fragments per kilobase of transcript per million mapped reads (FPKM)-normalized gene expression data from the ROSMAP cohort was log transformed and tested for correlation with methylation of PART EWAS CpG, TauAge feature CpGs, or PART-AD Classifier feature CpGs. Correlations were FDR-adjusted and CpG methylation:gene expression pairs with an absolute effect size value >= .2 and FDR < .0001 were filtered for further analysis. Only cases where both DNAm and RNA-sequencing data were available were included. To identify genes differentially expressed between AD-PART or Predicted AD-Predicted PART, linear Linearmodels were fit for each gene using the lmFit function from the Limma R package (3.58.1). The variance of a gene was stabilized using the eBayes function. DEGs were identified with a moderated t-test using the decideTests function with default parameters. To identify genes associated with p-tau pathology, gene expression for each gene was regressed on log transformed p-tau using the lm() function and genes with an FDR<.05 were considered for further analyses. All gene ontology analyses were performed using Enrichr[86-88].

Statistical testing (Predicted PART vs. Predicted AD): Standard t-tests were performed using the t.test function (stats 4.4.0) between Predicted PART and Predicted AD to compare mean TauAge, NFTs (hippocampal and midfrontal), neuritic plaques (midfrontal, total) and MMSE. Multiple testing was corrected using the FDR method.

Acknowledgements

We wish to thank all the individual study volunteers, tissue donors, and caregivers with whom this work would not be possible. This work was supported by funding from the National Institutes of Health (R01AG066152, P30AG072979, R35GM146978, UE5NS065745, T32AG076411, P01AG066597, P01AG084497) and Penn Institute on Aging. The results published here are in whole or in part based on data obtained from the AD Knowledge Portal. Study data were provided by the Rush Alzheimer's Disease Center, Rush University Medical Center, Chicago. Data collection was supported through funding by NIA grants P30AG10161, R01AG15819, R01AG17917, R01AG30146, R01AG36836, and the Illinois Department of Public Health (ROSMAP). Additional phenotypic data can be requested at www.radc.rush.edu. Brain banking and neuropathology assessments for the MSBB cohort were supported by NIH grants AG02219, AG05138, and MH064673 and the Department of Veterans Affairs VISN3 MIRECC.

Data Availability Statement

The data that support the findings of this study are available on reasonable request from the corresponding author. The data are not publicly available due to privacy or ethical restrictions.

Competing Interests Statement

The authors declare no relevant conflicts of interest.

Author Contributions

Conceptualization: CTM and WZ. Study design and methodology: DG, ARW, CTM, and WZ. Collection of data: JFC, KF, DAB, EBL Data Analysis: DG, ARW, ND. Manuscript writing: ARW, DG, CTM, and WZ. Manuscript editing: ARW, DG, ND, LPS, EBL, CTM, WZ. Resources and funding: CTM and WZ.

REFERENCES

1 Bouras, C., Hof, P. R. & Morrison, J. H. Neurofibrillary tangle densities in the hippocampal formation in a non-demented population define subgroups of patients with differential early pathologic changes. *Neuroscience letters.* **153**, 131-135 (1993). https://doi.org/10.1016/0304-3940(93)90305-5

2 Braak, H., Thal, D. R., Ghebremedhin, E. & Del Tredici, K. Stages of the Pathologic Process in Alzheimer Disease: Age Categories From 1 to 100 Years. *Journal of Neuropathology & Experimental Neurology* **70**, 960-969 (2011). https://doi.org/10.1097/nen.0b013e318232a379

3 Sonnen, J. A. Ecology of the Aging Human Brain. *Archives of Neurology* **68**, 1049 (2011). https://doi.org/10.1001/archneurol.2011.157

4 Ganz, A. B. *et al.* Neuropathology and cognitive performance in self-reported cognitively healthy centenarians. *Acta Neuropathol Commun* **6**, 64 (2018). https://doi.org/10.1186/s40478-018-0558-5

5 Cholerton, B. *et al.* Neuropathologic Burden and Dementia in Nonagenarians and Centenarians: Comparison of 2 Community-Based Cohorts. *Neurology* **102**, e208060 (2024). https://doi.org/10.1212/WNL.0000000000208060

6 Crary, J. F. *et al.* Primary age-related tauopathy (PART): a common pathology associated with human aging. *Acta Neuropathologica* **128**, 755-766 (2014). https://doi.org/10.1007/s00401-014-1349-0

7 Jefferson-George, K. S., Wolk, D. A., Lee, E. B. & Mcmillan, C. T. Cognitive decline associated with pathological burden in primary age-related tauopathy. *Alzheimer's & Dementia* **13**, 1048-1053 (2017). https://doi.org/10.1016/j.jalz.2017.01.028

8 Braak, H. & Braak, E. Neuropathological stageing of Alzheimer-related changes. *Acta neuropathologica.* **82**, 239-259 (1991). https://doi.org/10.1007/BF00308809

9 Jellinger, K. A. *et al.* PART, a distinct tauopathy, different from classical sporadic Alzheimer disease. *Acta Neuropathologica* **129**, 757-762 (2015). https://doi.org/10.1007/s00401-015-1407-2

10 Wang, X. *et al.* Primary age-related tauopathy in a Chinese cohort. *Journal of Zhejiang University-SCIENCE B* **21**, 256-262 (2020). https://doi.org/10.1631/jzus.b1900262

11 Savola, S. *et al.* Primary age-related tauopathy in a Finnish population-based study of the oldest old (Vantaa 85+). *Neuropathol Appl Neurobiol* **48**, e12788 (2022). https://doi.org/10.1111/nan.12788

12 Nelson, P. T. *et al.* Brains With Medial Temporal Lobe Neurofibrillary Tangles But No Neuritic Amyloid Plaques Are a Diagnostic Dilemma But May Have Pathogenetic Aspects Distinct From Alzheimer Disease. *Journal of Neuropathology & Experimental Neurology* **68**, 774-784 (2009). https://doi.org/10.1097/nen.0b013e3181aacbe9

13 Mungas, D., Tractenberg, R., Schneider, J. A., Crane, P. K. & Bennett, D. A. A 2-process model for neuropathology of Alzheimer's disease. *Neurobiology of Aging* **35**, 301-308 (2014). https://doi.org/10.1016/j.neurobiolaging.2013.08.007

14 Mcmillan, C. T. *et al.* Alzheimer's genetic risk is reduced in primary age-related tauopathy: a potential model of resistance? *Annals of Clinical and Translational Neurology* **5**, 927-934 (2018). https://doi.org/10.1002/acn3.581

15 Farrell, K. *et al.* Genome-wide association study and functional validation implicates JADE1 in tauopathy. *Acta Neuropathologica* **143**, 33-53 (2022). https://doi.org/10.1007/s00401-021-02379-z

16 Montine, T. J. *et al.* National Institute on Aging–Alzheimer's Association guidelines for the neuropathologic assessment of Alzheimer's disease: a practical approach. *Acta Neuropathologica* **123**, 1-11 (2012). https://doi.org/10.1007/s00401-011-0910-3

17 Crary, J. Primary age-related tauopathy and the amyloid cascade hypothesis: the exception that proves the rule? *Journal of Neurology and Neuromedicine* **1**, 53-57 (2016). https://doi.org/10.29245/2572.942x/2016/6.1059

18 De Jager, P. L. *et al.* Alzheimer's disease: early alterations in brain DNA methylation at ANK1, BIN1, RHBDF2 and other loci. *Nat Neurosci* **17**, 1156-1163 (2014). https://doi.org/10.1038/nn.3786

19 Smith, R. G. *et al.* A meta-analysis of epigenome-wide association studies in Alzheimer's disease highlights novel differentially methylated loci across cortex. *Nature Communications* **12** (2021). https://doi.org/10.1038/s41467-021-23243-4

20 Shireby, G. *et al.* DNA methylation signatures of Alzheimer's disease neuropathology in the cortex are primarily driven by variation in non-neuronal cell-types. *Nature Communications* **13** (2022). https://doi.org/10.1038/s41467-022-33394-7

21 Lang, A.-L. *et al.* Methylation differences in Alzheimer's disease neuropathologic change in the aged human brain. *Acta Neuropathologica Communications* **10** (2022). https://doi.org/10.1186/s40478-022-01470-0

22 Li, Z. *et al.* Differential DNA methylation in the brain as potential mediator of the association between traffic-related PM(2.5) and neuropathology markers of Alzheimer's disease. *Alzheimers Dement* **20**, 2538-2551 (2024). https://doi.org/10.1002/alz.13650

23 Zhang, J. *et al.* Integrative multi-omics analysis reveals the critical role of the <scp>PBXIP1</scp> gene in Alzheimer's disease. *Aging Cell* (2023). https://doi.org/10.1111/acel.14044

24 Thrush, K. L. *et al.* Aging the brain: multi-region methylation principal component based clock in the context of Alzheimer's disease. *Aging (Albany NY)* **14**, 5641-5668 (2022). https://doi.org/10.18632/aging.204196

25 Shireby, G. L. *et al.* Recalibrating the epigenetic clock: implications for assessing biological age in the human cortex. *Brain* **143**, 3763-3775 (2020). https://doi.org/10.1093/brain/awaa334

26 Bell, C. G. *et al.* DNA methylation aging clocks: challenges and recommendations. *Genome Biology* **20** (2019). https://doi.org/10.1186/s13059-019-1824-y

27 Mostafavi, S. *et al.* A molecular network of the aging human brain provides insights into the pathology and cognitive decline of Alzheimer's disease. *Nature Neuroscience* **21**, 811-819 (2018). https://doi.org/10.1038/s41593-018-0154-9

28 Moore, L. D., Le, T. & Fan, G. DNA Methylation and Its Basic Function. *Neuropsychopharmacology* **38**, 23-38 (2013). https://doi.org/10.1038/npp.2012.112

29 Domcke, S. *et al.* Competition between DNA methylation and transcription factors determines binding of NRF1. *Nature* **528**, 575-579 (2015). https://doi.org/10.1038/nature16462

30 Horvath, S. Erratum to: DNA methylation age of human tissues and cell types. *Genome Biol* **16**, 96 (2015). https://doi.org/10.1186/s13059-015-0649-6

31 Horvath, S. DNA methylation age of human tissues and cell types. *Genome Biol* **14**, R115 (2013). https://doi.org/10.1186/gb-2013-14-10-r115

32 Zhou, W. & Reizel, Y. On correlative and causal links of replicative epimutations. *Trends Genet* (2024). https://doi.org/10.1016/j.tig.2024.08.008

33 Duyckaerts, C. *et al.* PART is part of Alzheimer disease. *Acta Neuropathologica* **129**, 749-756 (2015). https://doi.org/10.1007/s00401-015-1390-7

34 Gourmaud, S. *et al.* Alzheimer-like amyloid and tau alterations associated with cognitive deficit in temporal lobe epilepsy. *Brain* **143**, 191-209 (2020). https://doi.org/10.1093/brain/awz381

35 Iida, M. A. *et al.* Predictors of cognitive impairment in primary age-related tauopathy: an autopsy study. *Acta Neuropathologica Communications* **9** (2021). https://doi.org/10.1186/s40478-021-01233-3

36 Josephs, K. A. *et al.* Tau aggregation influences cognition and hippocampal atrophy in the absence of beta-amyloid: a clinico-imaging-pathological study of primary age-related tauopathy (PART). *Acta Neuropathol* **133**, 705-715 (2017). https://doi.org/10.1007/s00401-017-1681-2

37 Teylan, M. *et al.* Cognitive trajectory in mild cognitive impairment due to primary age-related tauopathy. *Brain* **143**, 611-621 (2020). https://doi.org/10.1093/brain/awz403

38 Smith, R. G. *et al.* Elevated DNA methylation across a 48-kb region spanning the HOXA gene cluster is associated with Alzheimer's disease neuropathology. *Alzheimers Dement* **14**, 1580-1588 (2018). https://doi.org/10.1016/j.jalz.2018.01.017

39 Mesías, R. E. *et al.* Development and cadherin-mediated control of prefrontal corticostriatal projections in mice. *iScience* **26**, 108002 (2023). https://doi.org/10.1016/j.isci.2023.108002

40 Li, L. *et al.* Regulation of maternal behavior and offspring growth by paternally expressed Peg3. *Science* **284**, 330-333 (1999). https://doi.org/10.1126/science.284.5412.330

41 Fukushi, D. *et al.* <scp>R3HDM1</scp> haploinsufficiency is associated with mild intellectual disability. *American Journal of Medical Genetics Part A* **185**, 1776-1786 (2021). https://doi.org/10.1002/ajmg.a.62173

42 Cotney, J. *et al.* The autism-associated chromatin modifier CHD8 regulates other autism risk genes during human neurodevelopment. *Nature Communications* **6**, 6404 (2015). https://doi.org/10.1038/ncomms7404

43 Mulder, R. H. *et al.* Epigenome-wide change and variation in DNA methylation in childhood: trajectories from birth to late adolescence. *Hum Mol Genet* **30**, 119-134 (2021). https://doi.org/10.1093/hmg/ddaa280

44 Megraw, M. *et al.* Isoform specific gene auto-regulation via miRNAs: a case study on miR-128b and ARPP-21. *Theoretical Chemistry Accounts* **125**, 593-598 (2010). https://doi.org/10.1007/s00214-009-0647-4

45 Ching, A.-S. & Ahmad-Annuar, A. A Perspective on the Role of microRNA-128 Regulation in Mental and Behavioral Disorders. *Frontiers in Cellular Neuroscience* **9** (2015). https://doi.org/10.3389/fncel.2015.00465

46 Marangi, G., Orteschi, D., Milano, V., Mancano, G. & Zollino, M. Interstitial deletion of 3p22.3p22.2 encompassing ARPP21 and CLASP2 is a potential pathogenic factor for a syndromic form of intellectual disability: A co-morbidity model with additional copy number variations in a large family. *American Journal of Medical Genetics Part A* **161**, 2890-2893 (2013). https://doi.org/10.1002/ajmg.a.36257

47 Tan, C. L. *et al.* MicroRNA-128 Governs Neuronal Excitability and Motor Behavior in Mice. *Science* **342**, 1254-1258 (2013). https://doi.org/10.1126/science.1244193

48 Hou, Y. *et al.* Ageing as a risk factor for neurodegenerative disease. *Nature Reviews Neurology* **15**, 565-581 (2019). https://doi.org/10.1038/s41582-019-0244-7

49 Meftah, S. & Gan, J. Alzheimer's disease as a synaptopathy: Evidence for dysfunction of synapses during disease progression. *Frontiers in Synaptic Neuroscience* **15** (2023). https://doi.org/10.3389/fnsyn.2023.1129036

50 Tzioras, M., Mcgeachan, R. I., Durrant, C. S. & Spires-Jones, T. L. Synaptic degeneration in Alzheimer disease. *Nature Reviews Neurology* **19**, 19-38 (2023). https://doi.org/10.1038/s41582-022-00749-z

51 Morrison, J. H. & Baxter, M. G. The ageing cortical synapse: hallmarks and implications for cognitive decline. *Nature Reviews Neuroscience* **13**, 240-250 (2012). https://doi.org/10.1038/nrn3200

52 Petralia, R. S., Mattson, M. P. & Yao, P. J. Communication breakdown: The impact of ageing on synapse structure. *Ageing Research Reviews* **14**, 31-42 (2014). https://doi.org/10.1016/j.arr.2014.01.003

53 Frohlich, A. S. *et al.* Single-nucleus transcriptomic profiling of human orbitofrontal cortex reveals convergent effects of aging and psychiatric disease. *Nat Neurosci* **27**, 2021-2032 (2024). https://doi.org/10.1038/s41593-024-01742-z

54 Ling, E. *et al.* A concerted neuron-astrocyte program declines in ageing and schizophrenia. *Nature* **627**, 604-611 (2024). https://doi.org/10.1038/s41586-024-07109-5

55 Huijbers, W. *et al.* Tau Accumulation in Clinically Normal Older Adults Is Associated with Hippocampal Hyperactivity. *The Journal of Neuroscience* **39**, 548-556 (2019). https://doi.org/10.1523/jneurosci.1397-18.2018

56 Nguyen, T. A., Lehr, A. W. & Roche, K. W. Neuroligins and Neurodevelopmental Disorders: X-Linked Genetics. *Frontiers in Synaptic Neuroscience* **12** (2020). https://doi.org/10.3389/fnsyn.2020.00033

57 Ichtchenko, K., Nguyen, T. & Südhof, T. C. Structures, Alternative Splicing, and Neurexin Binding of Multiple Neuroligins. *Journal of Biological Chemistry* **271**, 2676-2682 (1996). https://doi.org/10.1074/jbc.271.5.2676

58 Yan, J. *et al.* Analysis of the neuroligin 4Y gene in patients with autism. *Psychiatric genetics.* **18**, 204-207 (2008). https://doi.org/10.1097/YPG.0b013e3282fb7fe6

59 Du, W. *et al.* Kinesin 1 Drives Autolysosome Tubulation. *Developmental Cell* **37**, 326-336 (2016). https://doi.org/https://doi.org/10.1016/j.devcel.2016.04.014

60 Correia, S. C., Perry, G. & Moreira, P. I. Mitochondrial traffic jams in Alzheimer's disease - pinpointing the roadblocks. *Biochimica et Biophysica Acta (BBA) - Molecular Basis of Disease* **1862**, 1909-1917 (2016). https://doi.org/https://doi.org/10.1016/j.bbadis.2016.07.010

61 Selvarasu, K. *et al.* Reduction of kinesin I heavy chain decreases tau hyperphosphorylation, aggregation, and memory impairment in Alzheimer's disease and tauopathy models. *Front Mol Biosci* **9**, 1050768 (2022). https://doi.org/10.3389/fmolb.2022.1050768

62 Williams, J. B., Cao, Q. & Yan, Z. Transcriptomic analysis of human brains with Alzheimer's disease reveals the altered expression of synaptic genes linked to cognitive deficits. *Brain Communications* **3** (2021). https://doi.org/10.1093/braincomms/fcab123

63 Li, H. *et al.* Identification of the molecular subgroups in Alzheimer's disease by transcriptomic data. *Frontiers in Neurology* **13** (2022). https://doi.org/10.3389/fneur.2022.901179

64 Crist, A. M. *et al.* Transcriptomic analysis to identify genes associated with selective hippocampal vulnerability in Alzheimer's disease. *Nature Communications* **12** (2021). https://doi.org/10.1038/s41467-021-22399-3

65 Otero-Garcia, M. *et al.* Molecular signatures underlying neurofibrillary tangle susceptibility in Alzheimer's disease. *Neuron* **110**, 2929-2948.e2928 (2022). https://doi.org/10.1016/j.neuron.2022.06.021

66 Chen, W.-T. *et al.* Spatial Transcriptomics and In Situ Sequencing to Study Alzheimer's Disease. *Cell* **182**, 976-991.e919 (2020). https://doi.org/10.1016/j.cell.2020.06.038

67 Rexach, J. E. *et al.* Tau Pathology Drives Dementia Risk-Associated Gene Networks toward Chronic Inflammatory States and Immunosuppression. *Cell Reports* **33**, 108398 (2020). https://doi.org/10.1016/j.celrep.2020.108398

68 Sanchez-Rodriguez, L. M. *et al.* In-vivo neuronal dysfunction by Aβ and tau overlaps with brain-wide inflammatory mechanisms in Alzheimer's disease. *Frontiers in Aging Neuroscience* **16** (2024). https://doi.org/10.3389/fnagi.2024.1383163

69 Mathys, H. *et al.* Single-cell transcriptomic analysis of Alzheimer's disease. *Nature* **570**, 332-337 (2019). https://doi.org/10.1038/s41586-019-1195-2

70 Caldwell, A. B. *et al.* Transcriptomic profiling of sporadic Alzheimer's disease patients. *Molecular Brain* **15** (2022). https://doi.org/10.1186/s13041-022-00963-2

71 Folstein, M. F., Robins, L. N. & Helzer, J. E. The Mini-Mental State Examination. *Arch Gen Psychiatry* **40**, 812 (1983). https://doi.org/10.1001/archpsyc.1983.01790060110016

72 Morris, J. C. The Clinical Dementia Rating (CDR): current version and scoring rules. *Neurology* **43**, 2412-2414 (1993). https://doi.org/10.1212/wnl.43.11.2412-a

73 Mirra, S. S. *et al.* The Consortium to Establish a Registry for Alzheimer's Disease (CERAD). Part II. Standardization of the neuropathologic assessment of Alzheimer's disease. *Neurology* **41**, 479-486 (1991). https://doi.org/10.1212/wnl.41.4.479

74 Walker, J. M. *et al.* Early Selective Vulnerability of the CA2 Hippocampal Subfield in Primary Age-Related Tauopathy. *J Neuropathol Exp Neurol* **80**, 102-111 (2021). https://doi.org/10.1093/jnen/nlaa153

75 Kovacs, G. G. *et al.* Aging-related tau astrogliopathy (ARTAG): harmonized evaluation strategy. *Acta Neuropathol* **131**, 87-102 (2016). https://doi.org/10.1007/s00401-015-1509-x

76 Bennett, D. A. & Launer, L. J. Longitudinal epidemiologic clinical-pathologic studies of aging and Alzheimer's disease. *Curr Alzheimer Res* **9**, 617-620 (2012). https://doi.org/10.2174/156720512801322645

77 Marx, G. A. *et al.* Histopathologic brain age estimation via multiple instance learning. *Acta Neuropathologica* **146**, 785-802 (2023). https://doi.org/10.1007/s00401-023-02636-3

78 Marx, G. A. *et al.* Artificial intelligence-derived neurofibrillary tangle burden is associated with antemortem cognitive impairment. *Acta Neuropathol Commun* **10**, 157 (2022). https://doi.org/10.1186/s40478-022-01457-x

79 Bennett, D. A. *et al.* Pathological changes in frontal cortex from biopsy to autopsy in Alzheimer's disease. *Neurobiology of Aging* **14**, 589-596 (1993). https://doi.org/https://doi.org/10.1016/0197-4580(93)90043-B

80 Zhou, W., Triche, T. J., Laird, P. W. & Shen, H. SeSAMe: reducing artifactual detection of DNA methylation by Infinium BeadChips in genomic deletions. *Nucleic Acids Research* (2018). https://doi.org/10.1093/nar/gky691

81 Luo, C. *et al.* Single-cell methylomes identify neuronal subtypes and regulatory elements in mammalian cortex. *Science* **357**, 600-604 (2017). https://doi.org/10.1126/science.aan3351

82 Lee, D. S. *et al.* Simultaneous profiling of 3D genome structure and DNA methylation in single human cells. *Nat Methods* **16**, 999-1006 (2019). https://doi.org/10.1038/s41592-019-0547-z

83 Luo, C. *et al.* Single nucleus multi-omics identifies human cortical cell regulatory genome diversity. *Cell Genom* **2** (2022). https://doi.org/10.1016/j.xgen.2022.100107

84 Wang, Y., Grant, O. A., Zhai, X., McDonald-Maier, K. D. & Schalkwyk, L. C. Insights into ageing rates comparison across tissues from recalibrating cerebellum DNA methylation clock. *Geroscience* **46**, 39-56 (2024). https://doi.org/10.1007/s11357-023-00871-w

85 Kuhn, M. Building Predictive Models in R Using the caret Package. *Journal of Statistical Software* **28**, 1 - 26 (2008). https://doi.org/10.18637/jss.v028.i05

86 Chen, E. Y. *et al.* Enrichr: interactive and collaborative HTML5 gene list enrichment analysis tool. *BMC Bioinformatics* **14**, 128 (2013). https://doi.org/10.1186/1471-2105-14-128

87 Kuleshov, M. V. *et al.* Enrichr: a comprehensive gene set enrichment analysis web server 2016 update. *Nucleic Acids Res* **44**, W90-97 (2016). https://doi.org/10.1093/nar/gkw377

88 Xie, Z. *et al.* Gene Set Knowledge Discovery with Enrichr. *Curr Protoc* **1**, e90 (2021). https://doi.org/10.1002/cpz1.90

Appendix

The PART working group: Jean-Paul Vonsattel (Department of Pathology and Cell Biology, Department of Neurology, and the Taub Institute for Research on Alzheimer's Disease and the Aging Brain, Columbia University Medical Center, New York, NY), Andy F. Teich (Department of Pathology and Cell Biology, Department of Neurology, and the Taub Institute for Research on Alzheimer's Disease and the Aging Brain, Columbia University Medical Center, New York, NY), Marla Gearing (Department of Pathology and Laboratory Medicine (Neuropathology) and Neurology, Emory University School of Medicine, Atlanta, GA), Jonathan Glass (Department of Pathology and Laboratory Medicine (Neuropathology) and Neurology, Emory University School of Medicine, Atlanta, GA), Juan C. Troncoso (Department of Pathology, Division of Neuropathology, Johns Hopkins University School of Medicine, Baltimore, MD), Matthew P. Frosch (Department of Neurology and Pathology, Harvard Medical School and Massachusetts General Hospital, Charlestown, MA), Bradley T. Hyman (Department of Neurology and Pathology, Harvard Medical School and Massachusetts General Hospital, Charlestown, MA), Melissa E. Murray (Department of Neuroscience, Mayo Clinic, Jacksonville, FL), Johannes Attems (Translational and Clinical Research Institute, Newcastle University, Newcastle upon Tyne, UK), Margaret E. Flanagan (Department of Pathology (Neuropathology), Northwestern Cognitive Neurology and Alzheimer Disease Center, Northwestern University Feinberg School of Medicine, Chicago, IL), Qinwen Mao (Department of Pathology (Neuropathology), Northwestern Cognitive Neurology and Alzheimer Disease Center, Northwestern University Feinberg School of Medicine, Chicago, IL), M-Marsel Mesulam (Department of Pathology (Neuropathology), Northwestern Cognitive Neurology and Alzheimer Disease Center, Northwestern University Feinberg School of Medicine, Chicago, IL), Sandra Weintraub (Department of Pathology (Neuropathology), Northwestern Cognitive Neurology and Alzheimer Disease Center, Northwestern University Feinberg School of Medicine, Chicago, IL), Randy L. Woltjer (Department of Pathology, Oregon Health Sciences University, Portland, OR), Thao Pham (Department of Pathology, Oregon Health Sciences University, Portland, OR), Julia Kofler (Department of Pathology [Neuropathology], University of Pittsburgh Medical Center, Pittsburgh, PA), Julie A. Schneider (Departments of Pathology [Neuropathology] and Neurological Sciences, Rush University Medical Center, Chicago, IL), Lei Yu (Departments of Pathology [Neuropathology] and Neurological Sciences, Rush University Medical Center, Chicago, IL), Dushyant P. Purohit (Department of Pathology, Neuropathology Brain Bank and Research CoRE, Icahn School of Medicine at Mount Sinai, James J. Peters VA Medical Center, New York, NY), Vahram Haroutunian (Department of Psychiatry, Alzheimer's Disease Research Center, James J. Peters VA Medical Center, Nash Department of Neuroscience, Ronald M. Loeb Center for Alzheimer's Disease, Friedman Brain Institute, Icahn School of Medicine at Mount Sinai, New York, NY), Patrick R. Hof (Nash Department of Neuroscience, Ronald M. Loeb Center for Alzheimer's Disease, Friedman Brain Institute, Icahn School of Medicine at Mount Sinai, New York, NY), Sam Gandy (Departments of Psychiatry and Neurology, Center for Cognitive Health, Alzheimer's Disease Research Center, James J. Peters VA Medical Center, Icahn School of Medicine at Mount Sinai, New York, NY and Department of Icahn School of Medicine at Mount Sinai, New York, NY), Mary Sano (Department of Psychiatry, Alzheimer's Disease Research Center, James J. Peters VA Medical Center, Icahn School of Medicine at Mount Sinai, New York, NY), Thomas G. Beach (Department of Neuropathology, Banner Sun Health Research Institute, Sun City, AZ), Wayne Poon (Department of Neurology, Department of Epidemiology, Institute for Memory Impairments and Neurological Disorders, UC Irvine, Irvine, CA), Claudia H. Kawas (Department of Neurology, Department of Neurobiology and Behavior, Institute for Memory Impairments and Neurological Disorders, UC Irvine, Irvine, CA), María M. Corrada (Department of Neurology, Department of Epidemiology, Institute for Memory Impairments and Neurological Disorders, UC Irvine, Irvine, CA), Robert A. Rissman (Department of Neurosciences University of California and the Veterans Affairs San Diego Healthcare System, La Jolla, San Diego, CA), Jeff Metcalf (Department of Neurosciences University of California and the Veterans Affairs San Diego Healthcare System, La Jolla, San Diego, CA), Sara Shuldberg (Department of Neurosciences University of California and the Veterans Affairs San Diego Healthcare System, La Jolla, San Diego, CA), Bahar Salehi (Department of Neurosciences University of California and the Veterans Affairs San Diego Healthcare System, La Jolla, San Diego, CA), Peter T. Nelson (Department of Pathology [Neuropathology] and Sanders-Brown Center on Aging, University of Kentucky, Lexington, KY), John Q. Trojanowski (Center for Neurodegenerative Disease Research, Department of Pathology and Laboratory Medicine, Perelman School of Medicine, University of Pennsylvania, Philadelphia, PA), Edward B. Lee (Center for Neurodegenerative Disease Research, Department of Pathology and Laboratory Medicine, Perelman School of Medicine, University of Pennsylvania, Philadelphia, PA), David A. Wolk (Department of Neurology, Perelman School of Medicine, University of Pennsylvania, Philadelphia, PA), Corey T. McMillan (Department of Neurology, Perelman School of Medicine, University of Pennsylvania, Philadelphia, PA), C. Dirk Keene (Department of Laboratory Medicine and Pathology, University of Medicine, Seattle, WA), Caitlin S. Latimer (Department of Laboratory Medicine and Pathology, University of Medicine, Seattle, WA), Thomas J. Montine (Department of Laboratory Medicine and Pathology, University of Medicine, Seattle, WA and Department of Pathology, Stanford University, Palo Alto, CA), Gabor G. Kovacs (Laboratory Medicine Program, Krembil Brain Institute, University Health Network, Toronto, ON, Canada, Tanz Centre for Research in Neurodegenerative Disease and Department of Laboratory Medicine and Pathobiology, University of Toronto, Toronto, Ontario, Canada, and Institute of Neurology, Medical University of Vienna, Vienna, Austria), Mirjam I. Lutz (Institute of Neurology, Medical University of Vienna, Vienna, Austria), Peter Fischer (Department of Psychiatry, Danube Hospital, Vienna, Austria), Richard J Perrin (Department of Pathology and Immunology, Department of Neurology, Knight Alzheimer Disease Research Center, Washington University School of Medicine, St. Louis, MO), Nigel J. Cairns (College of Medicine and Health, University of Exeter, Exeter, UK).

FIGURE 1

A

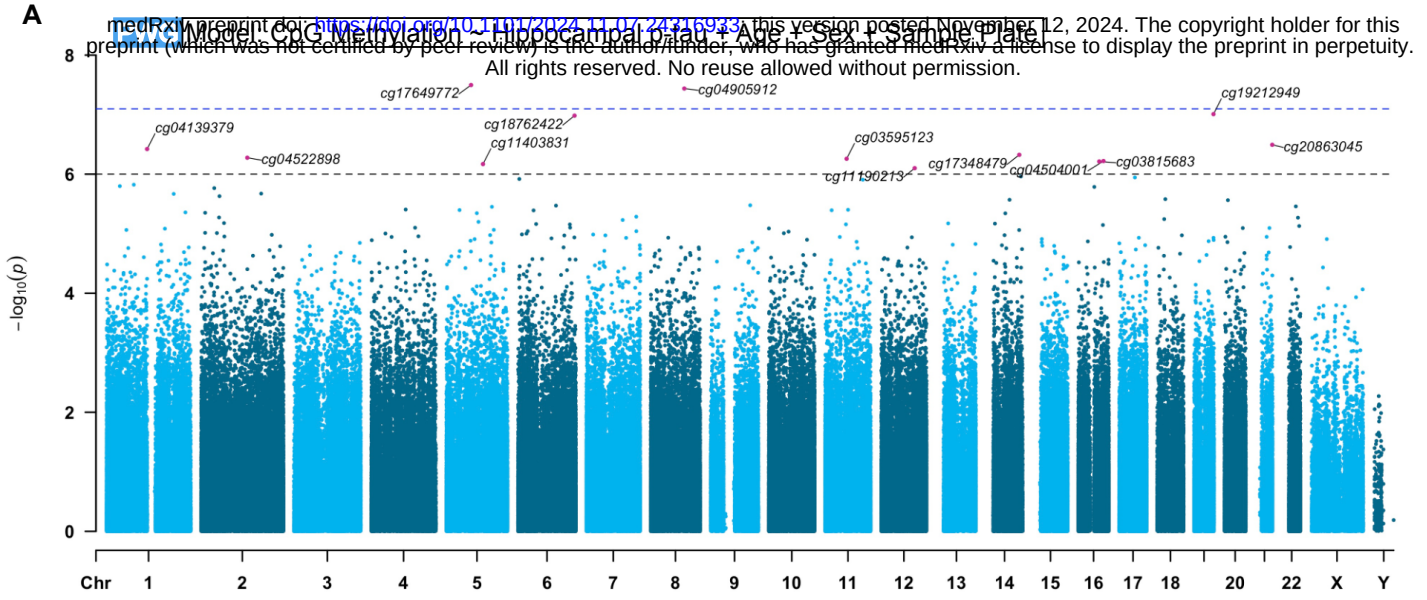

B

PWG EWAS (n=176)				ROSMAP (n=513)					
CpG	CpG ~ log(p-Tau) Effect Size	FDR	CpG Proximal Gene (10KB)	Methylation-Proximal Gene Exp Correlation (ROSMAP)	P	FDR	Gene ~ log(p-Tau) Effect Size	P	FDR
cg17649772	-0.05721	0.0128	ANKRA2	CpG not on HM450			-0.21004	0.24795	0.35126
cg17649772	-0.05721	0.0128	UTP15				-0.28974	0.11380	0.21496
cg04905912	-0.10131	0.0128		No proximal gene within 10KB					
cg18762422	-0.19215	0.0183	RPS6KA2	0.02339	0.59714	0.96490	0.05347	0.82275	0.82275
cg18762422	-0.19215	0.0183	MIR1913						
cg19212949	-0.04472	0.0183	AC006115.2	Expression data NA / 0					
cg19212949	-0.04472	0.0183	ZIM2						
cg19212949	-0.04472	0.0183	PEG3	-0.11446	0.00947	0.037881628	-0.20881	0.07226	0.15695
cg03595123	-0.09459	0.0392	RTN3*	0.09106	0.03924	0.09937	-0.17309	0.01637	0.05567
cg03815683	-0.05125	0.0392	CDH8	0.12926	0.00336	0.02016	-0.31494	0.00522	0.02959
cg04139379	-0.06454	0.0392	PHGDH*	CpG not on HM450			0.11062	0.35335	0.46207
cg04504001	-0.05951	0.0392	AC138627.1	0.02003	0.65090	0.96490	-0.15488	0.72596	0.77133
cg04504001	-0.05951	0.0392	PSMD7*	-0.00050	0.99104	0.99104	-0.31625	0.07342	0.15695
cg04504001	-0.05951	0.0392	AC009120.2	-0.00643	0.88449	0.96490	-0.09130	0.66052	0.74858
cg04504001	-0.05951	0.0392	AC009120.1	0.01713	0.69868	0.96490	0.22057	0.07386	0.15695
cg04504001	-0.05951	0.0392	AC009120.3	Expression data NA / 0					
cg04522898	-0.06836	0.0392	ZRANB3	0.09008	0.04140	0.09937	-0.79485	0.00042	0.00716
cg04522898	-0.06836	0.0392	R3HDM1	0.18551	0.00002	0.00028	-0.21534	0.00906	0.03850
cg17348479	-0.10813	0.0392	AL137786.1	0.00753	0.86491	0.96490	-0.44481	0.00123	0.01042
cg20863045	-0.11313	0.0392	PCBP3	CpG not on HM450			-0.09405	0.51425	0.62445
cg20863045	-0.11313	0.0392	AL133492.1	Expression data NA / 0					
cg11403831	-0.05541	0.0397	FER	-0.00964	0.82750	0.96490	0.47104	0.14856	0.25256
cg11190213	-0.05846	0.0429	LINC02453	CpG not on HM450			-0.42477	0.20586	0.31814

*Implicated in AD

C

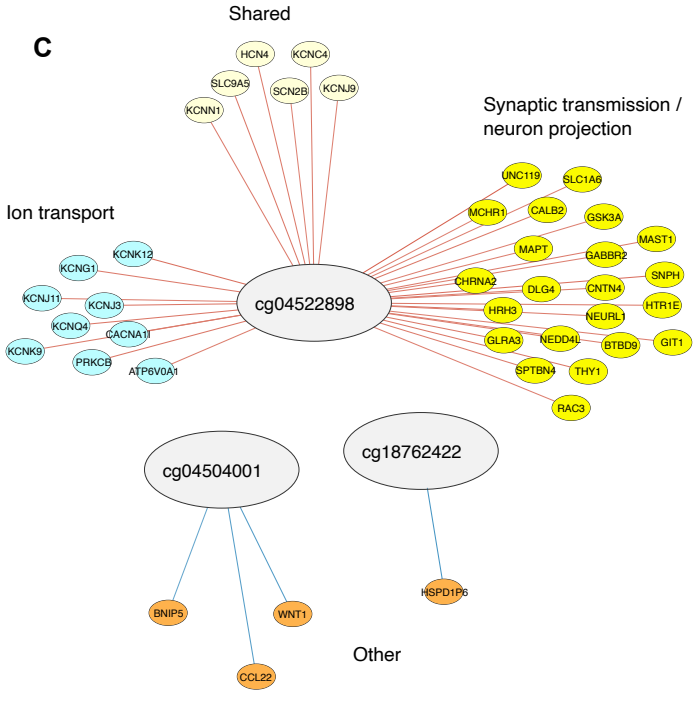

D

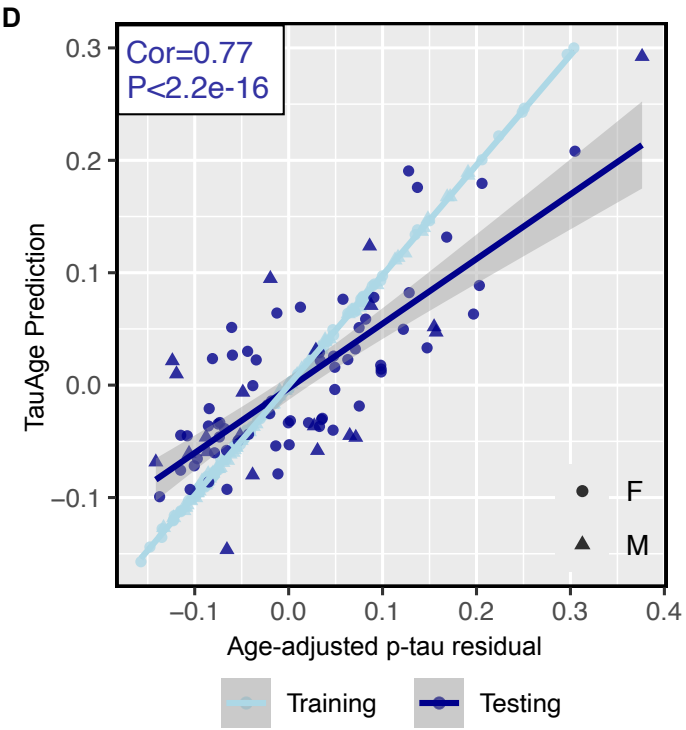

FIGURE 2

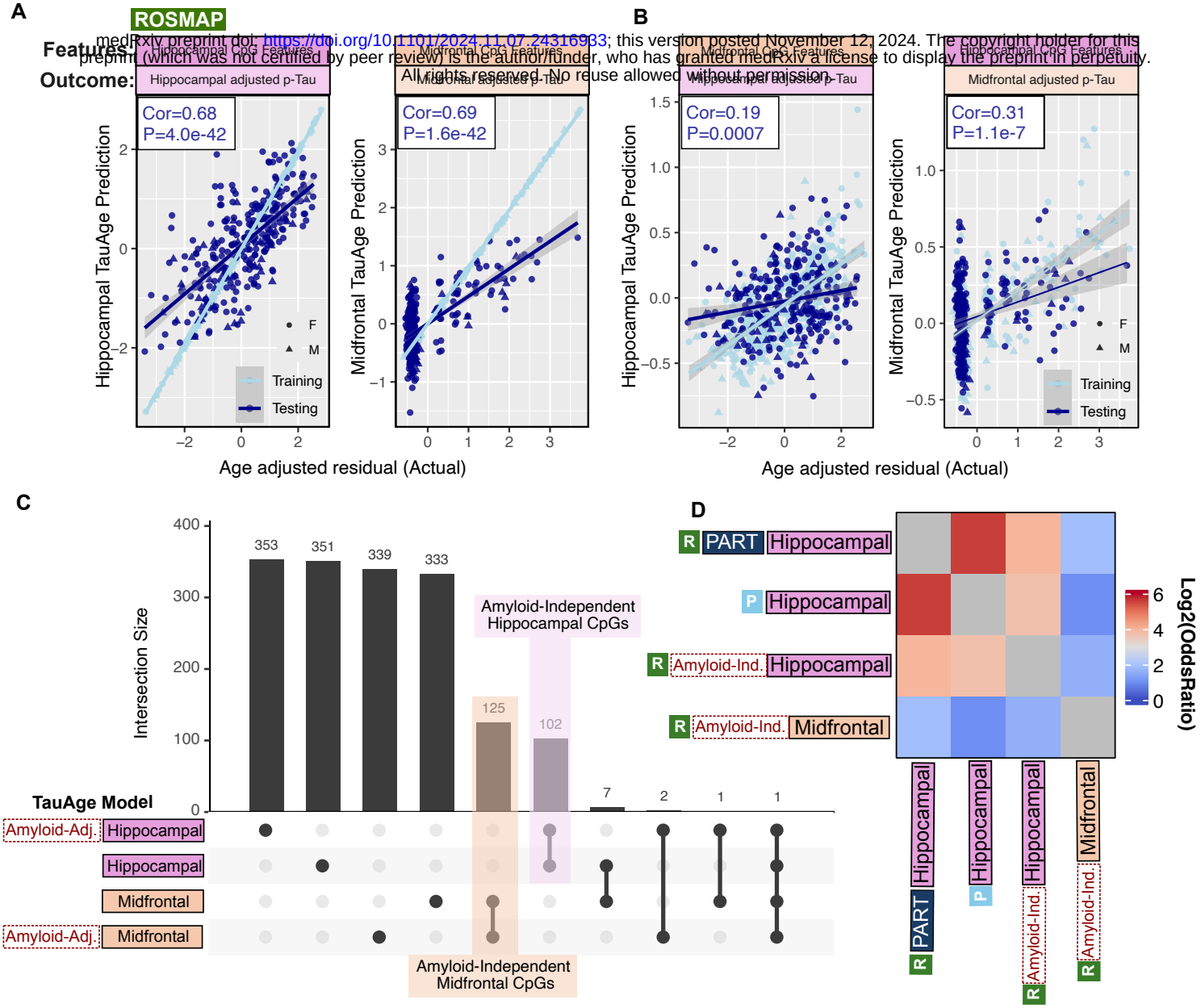

FIGURE 3

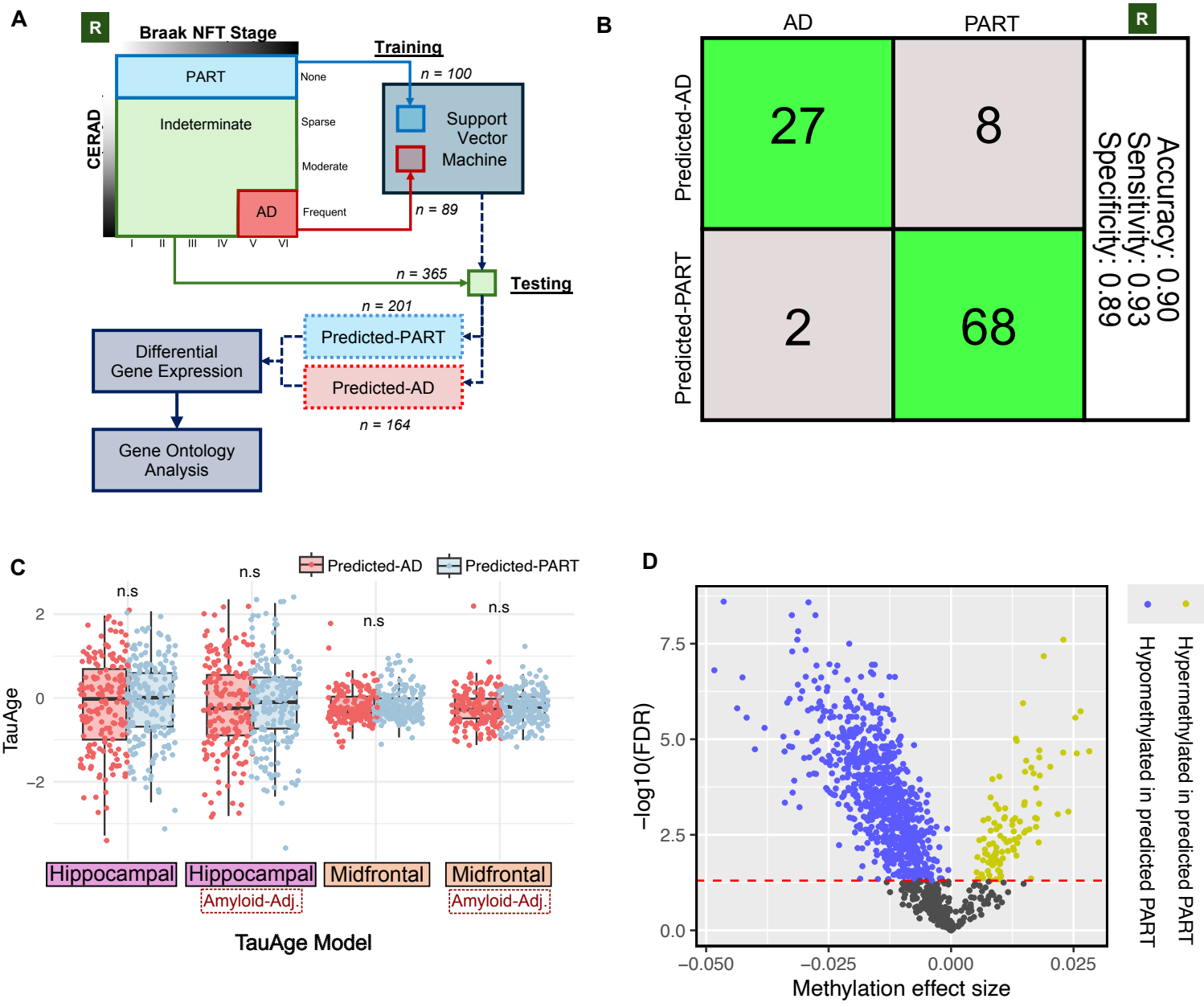

FIGURE 4

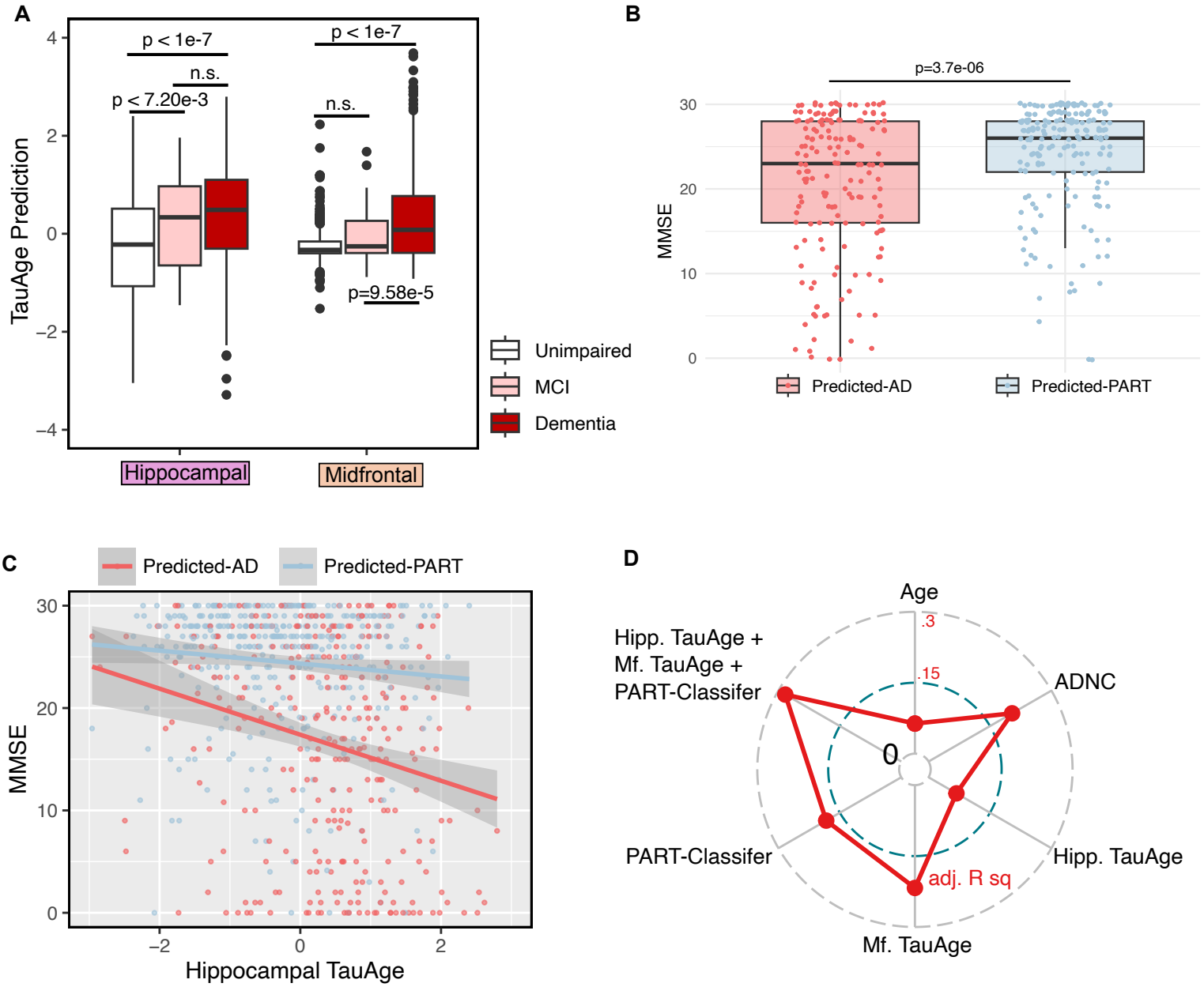

SUPPLEMENTAL TABLE 1

	PWG	ROSMAP				
	PART	Total	No Pathology	PART	Indeterminate	AD
Total	260	707	9	176	365	157
Sex (%)						
Female	152 (58%)	448 (63%)	3 (33%)	101 (57%)	228 (62%)	116 (74%)
Male	108 (42%)	259 (37%)	6 (67%)	75 (43%)	137 (38%)	41 (26%)
Age (%)						
51-60	4 (2%)	0 (0%)	0 (0%)	0 (0%)	0 (0%)	0 (0%)
61-70	9 (3%)	5 (1%)	1 (11%)	3 (2%)	1 (0%)	0 (0%)
71-80	45 (17%)	78 (11%)	4 (44%)	30 (17%)	38 (10%)	6 (4%)
81-90	99 (38%)	351 (50%)	4 (44%)	94 (53%)	179 (49%)	74 (47%)
>90	103 (40%)	273 (39%)	0 (0%)	49 (28%)	147 (40%)	77 (49%)

EXTENDED DATA FIGURE 1

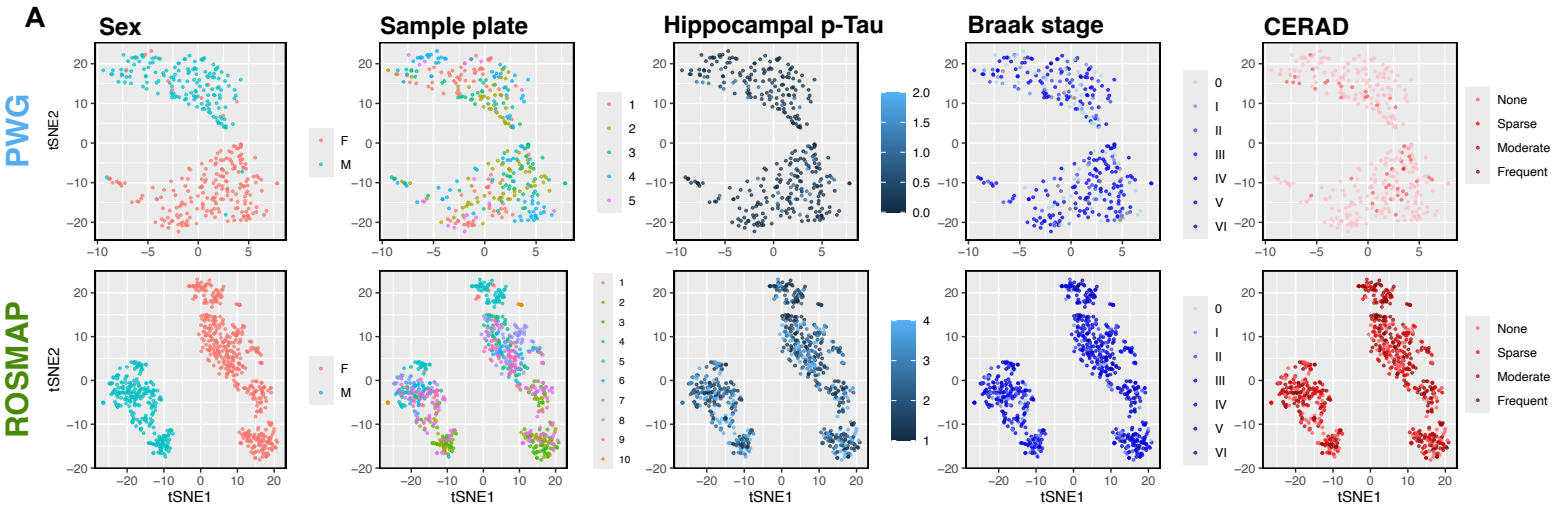

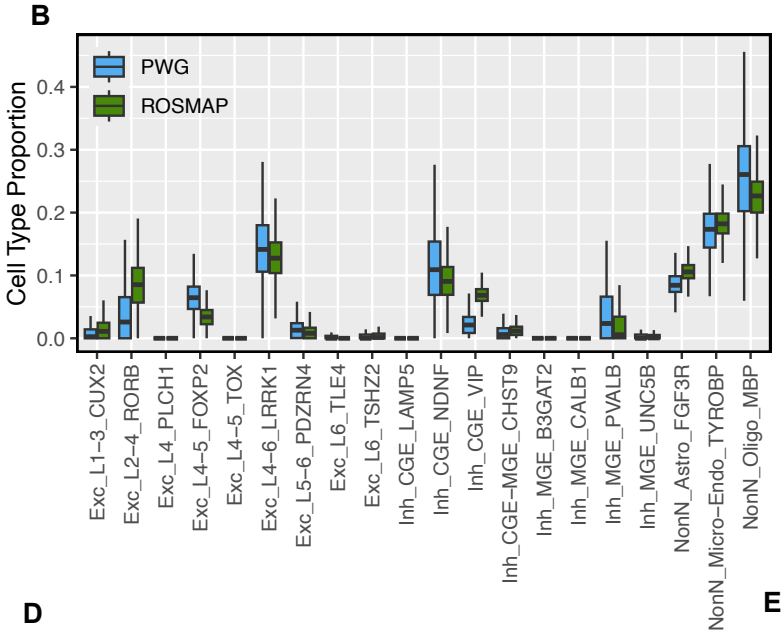

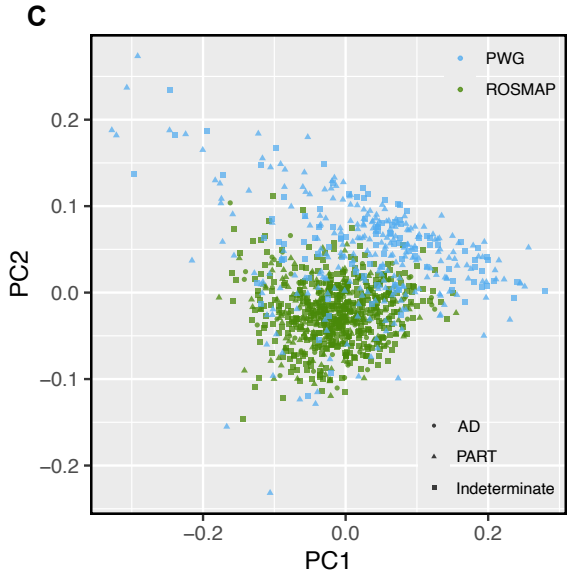

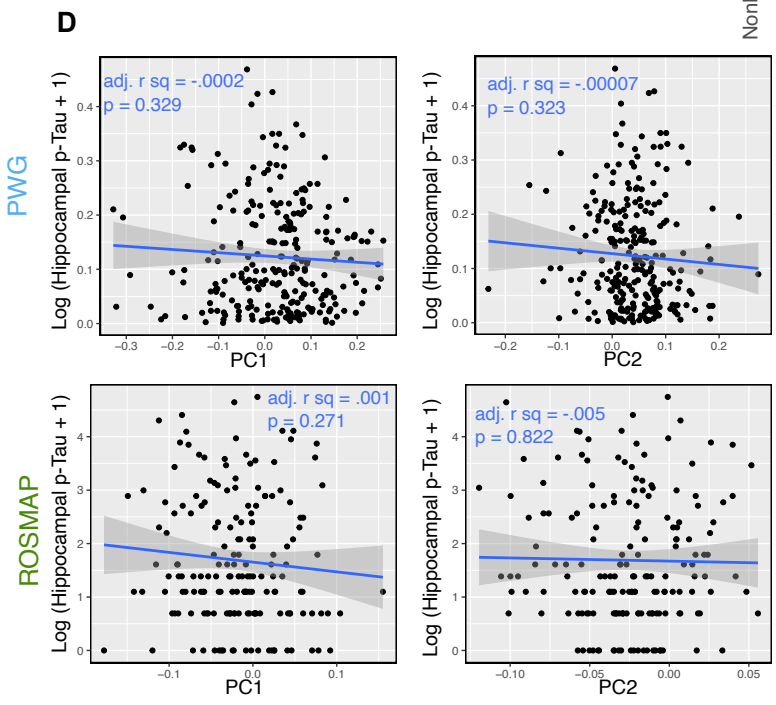

E

Model: Log (Hippocampal p-tau + 1) ~ Age + Sex + Cell Type Proportion			
CellType	Cell Type Coefficients		
	estimate	P	FDR
Exc_L1_3_CUX2	1.0818	0.02171	0.40589
Exc_L2_4_RORB	0.1630	0.18084	0.60279
Exc_L4_5_FOXP2	0.1240	0.57558	0.97032
Exc_L4_5_TOX	0.8250	0.63714	0.97032
Exc_L4_6_LRRK1	0.0179	0.87329	0.97032
Exc_L4_PLCH1	-1.3193	0.75646	0.97032
Exc_L5_6_PDZRN4	0.5294	0.14456	0.57822
Exc_L6_TLE4	0.2510	0.81081	0.97032
Exc_L6_TSHZ2	0.1982	0.82872	0.97032
Inh_CGE_LAMP5	-0.9975	0.45480	0.97032
Inh_CGE_MGE_CHST9	0.3834	0.47491	0.97032
Inh_CGE_NDNF	-0.0418	0.65974	0.97032
Inh_CGE_VIP	0.5493	0.08118	0.40589
Inh_MGE_B3GAT2	-1.4588	0.04519	0.40589
Inh_MGE_CALB1	-0.0065	0.97498	0.97805
Inh_MGE_PVALB	-0.0408	0.76213	0.97032
Inh_MGE_UNC5B	0.9846	0.22967	0.65621
NonN_Astro_FGF3R	0.1373	0.56920	0.97032
NonN_Micro_Endo_TYROBP	-0.0033	0.97805	0.97805
NonN_Oligo_MBP	-0.1277	0.07607	0.40589

EXTENDED DATA FIGURE 2

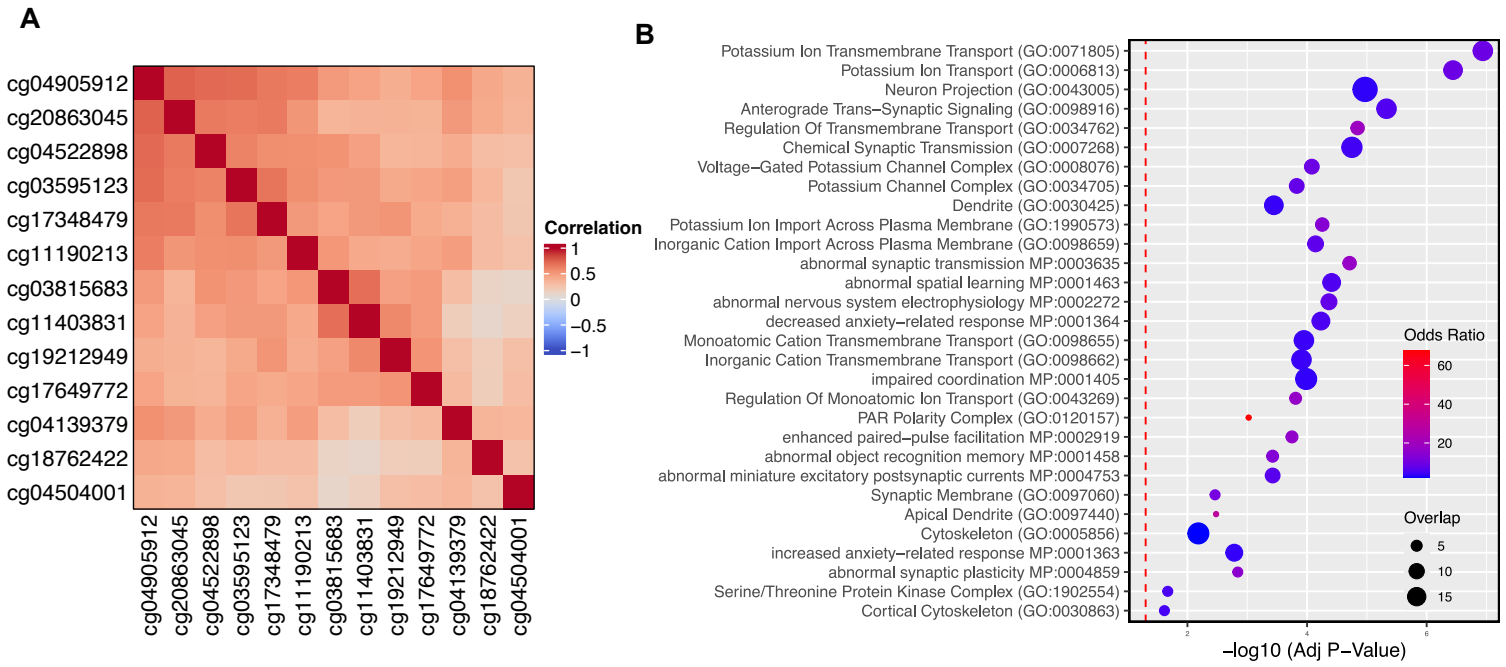

EXTENDED DATA FIGURE 3

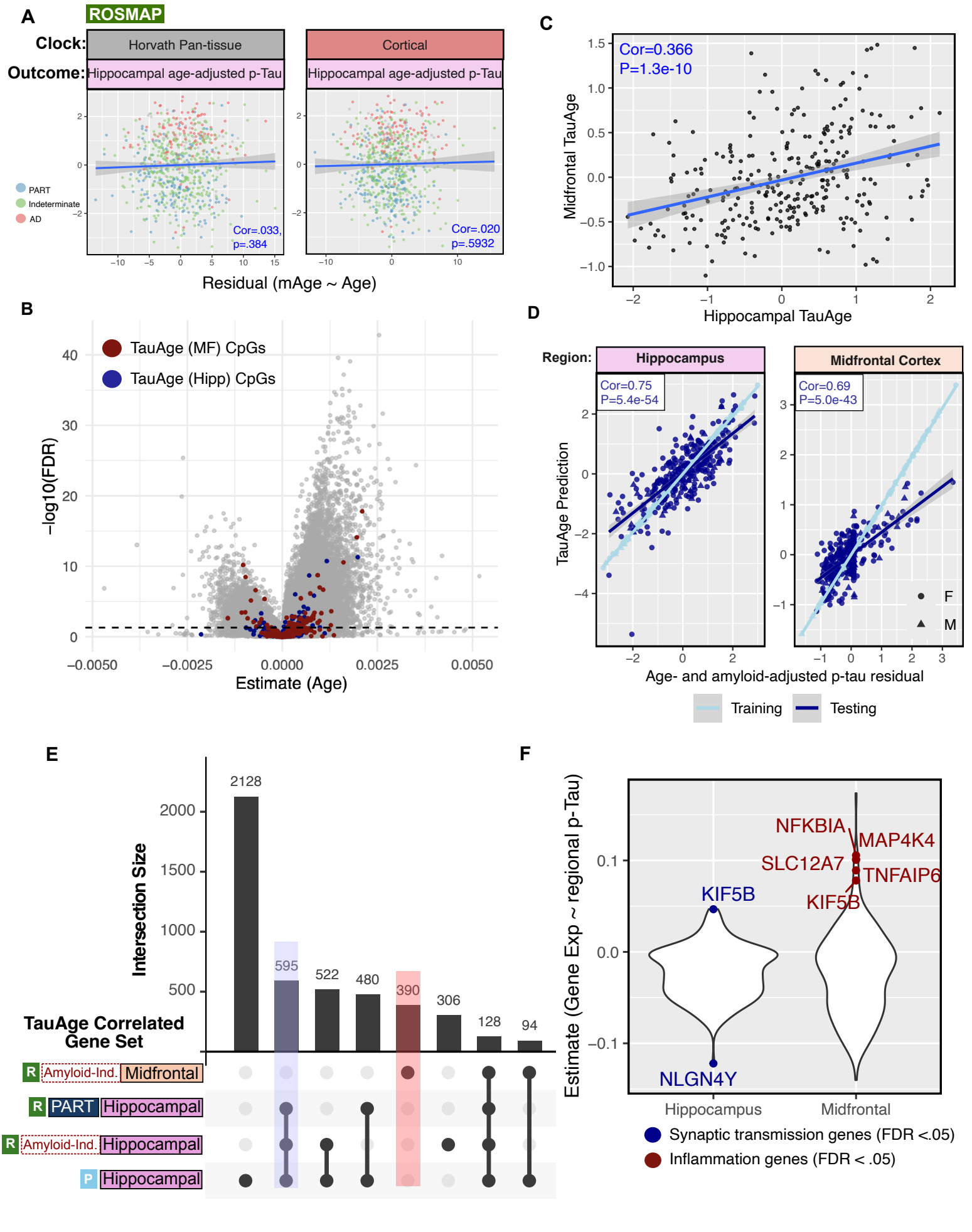

EXTENDED DATA FIGURE 4

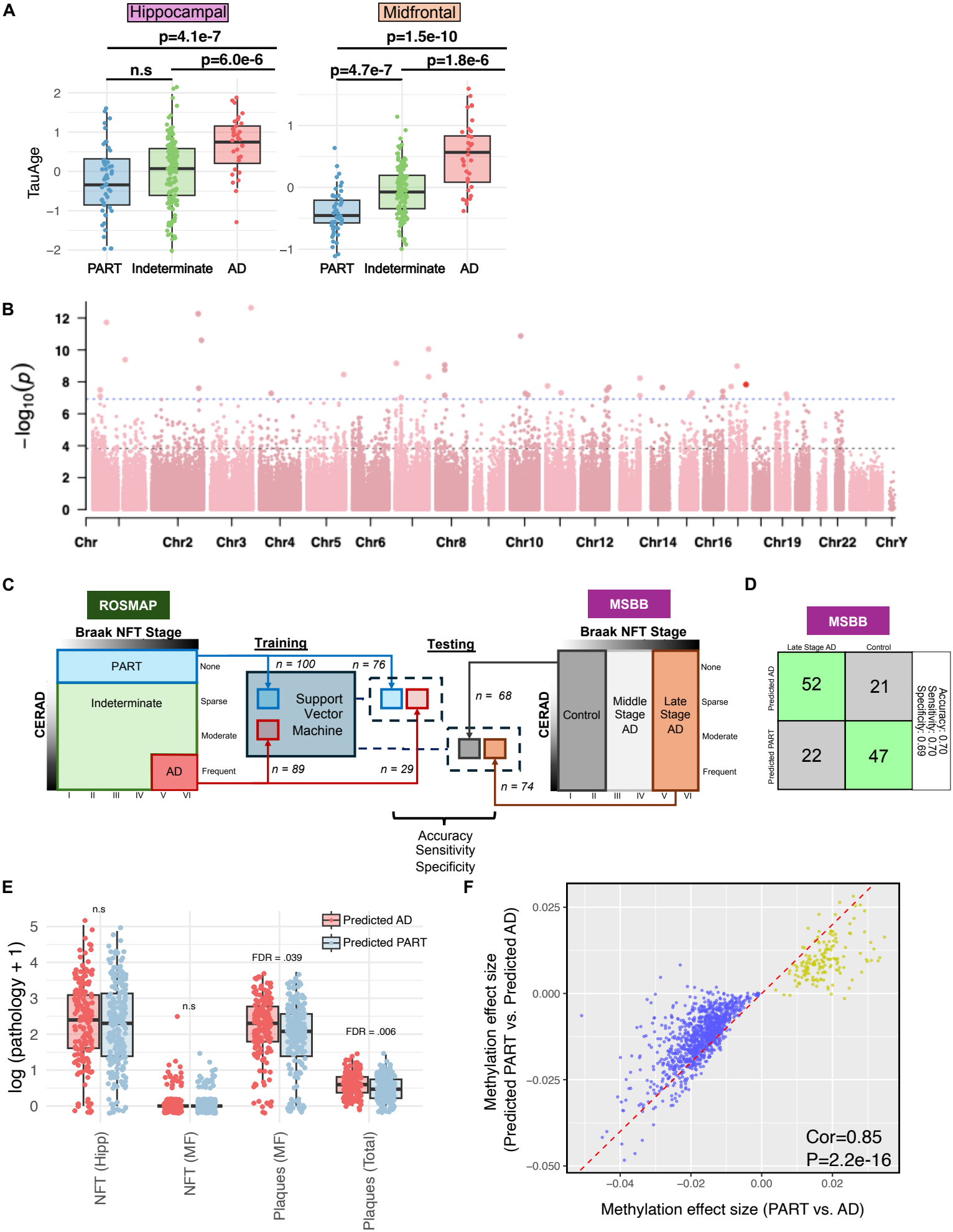

EXTENDED DATA FIGURE 5

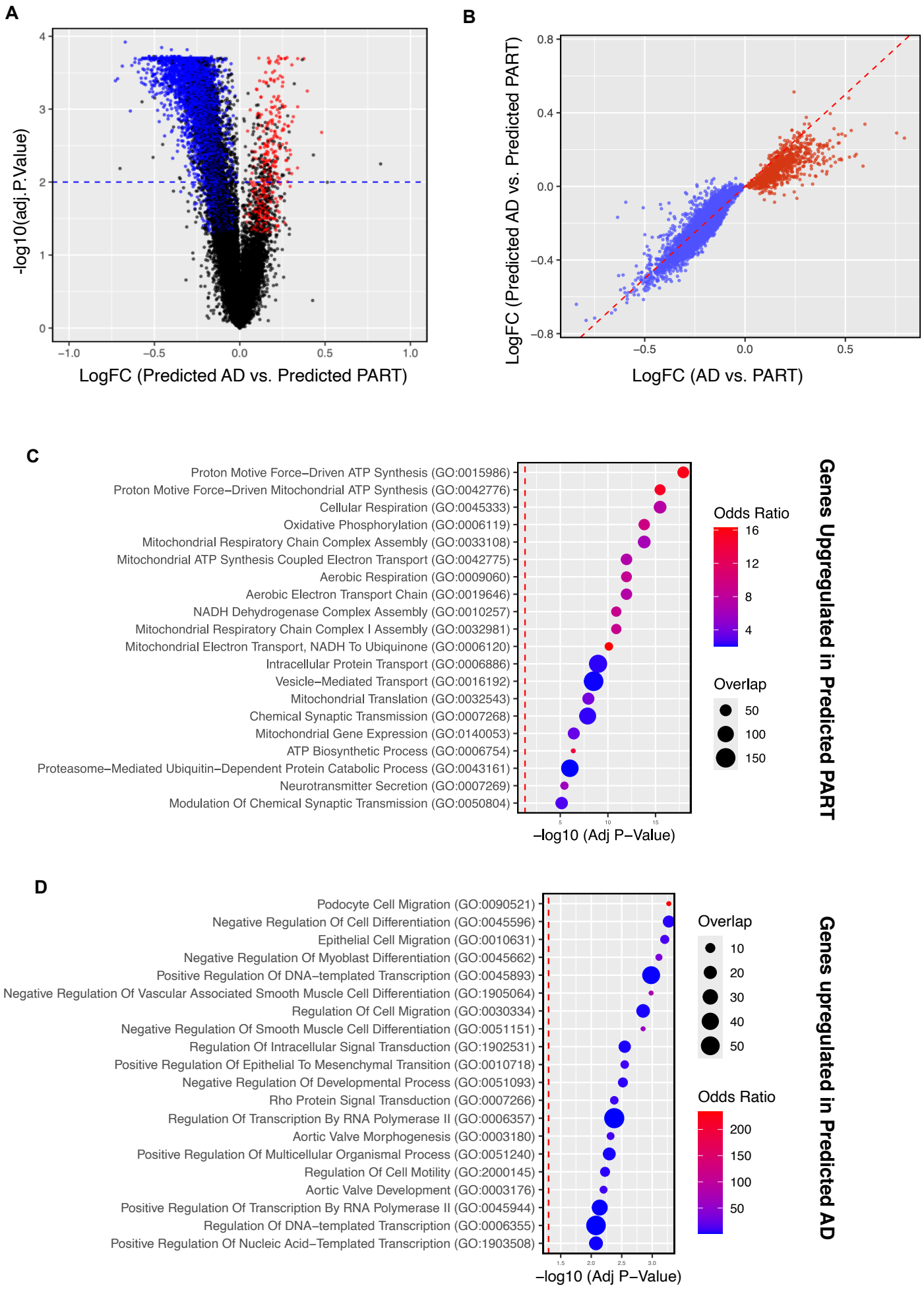

EXTENDED DATA FIGURE 1

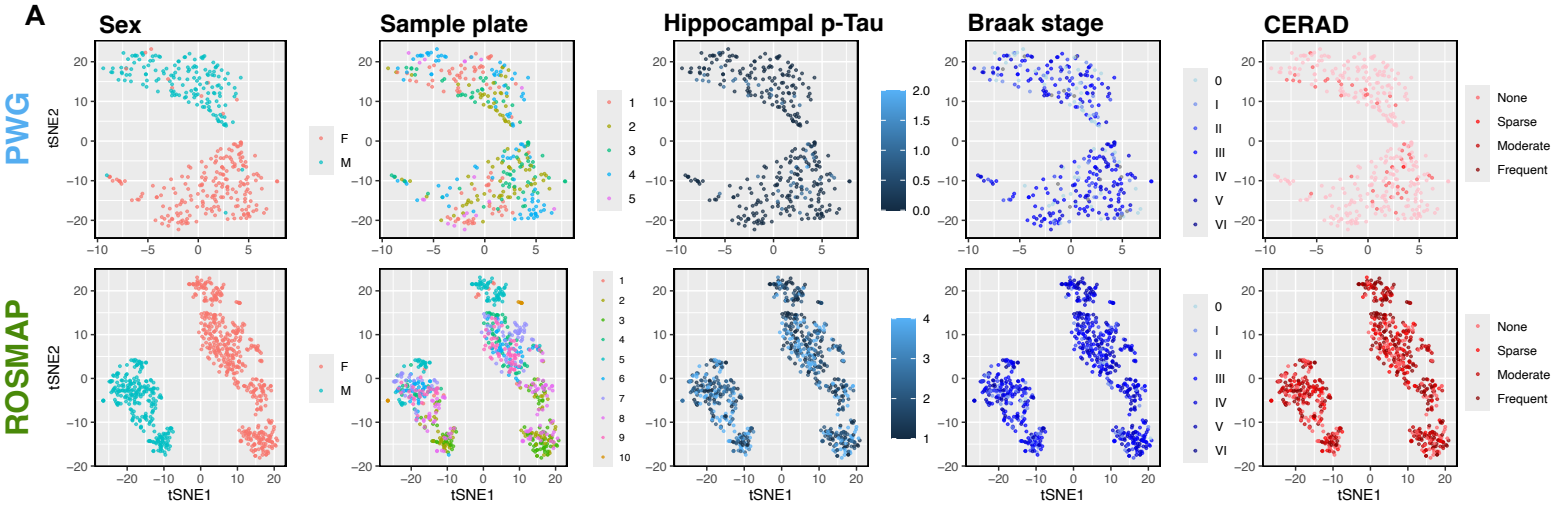

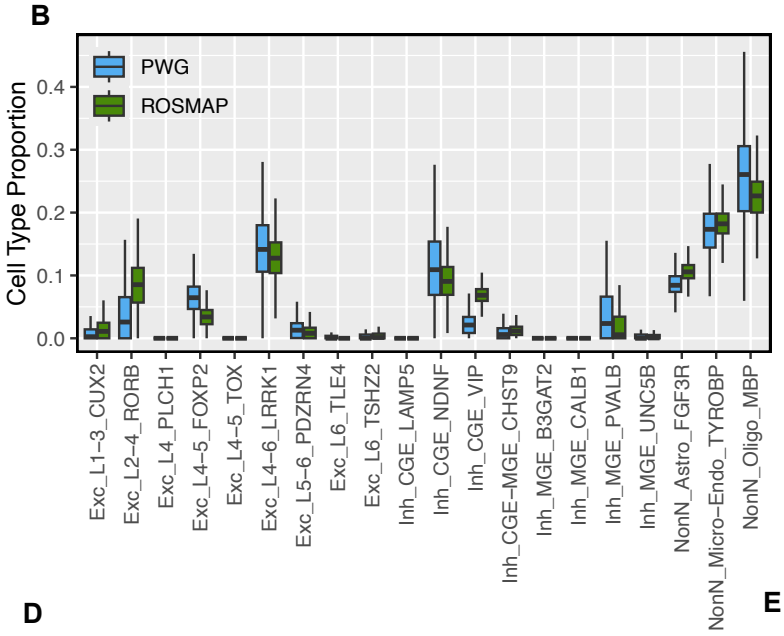

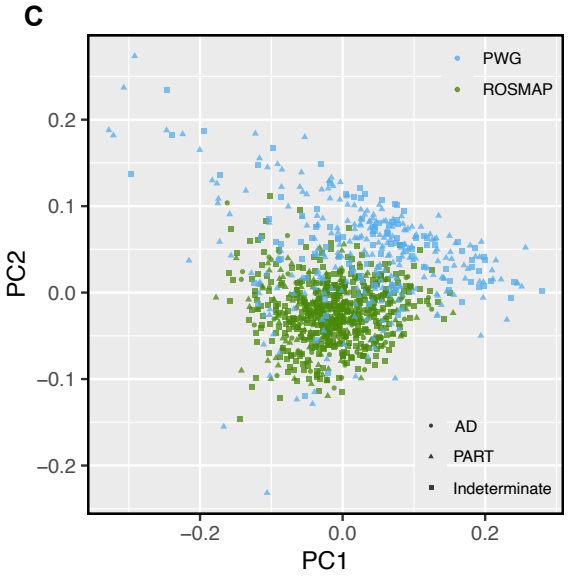

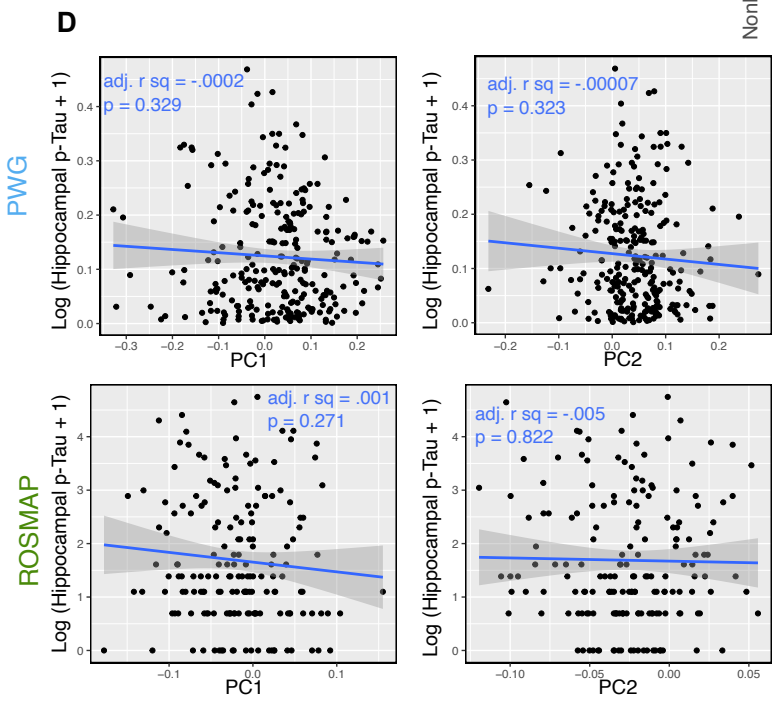

E

Model: Log (Hippocampal p-tau + 1) ~ Age + Sex + Cell Type Proportion			
CellType	Cell Type Coefficients		
	estimate	P	FDR
Exc_L1_3_CUX2	1.0818	0.02171	0.40589
Exc_L2_4_RORB	0.1630	0.18084	0.60279
Exc_L4_5_FOXP2	0.1240	0.57558	0.97032
Exc_L4_5_TOX	0.8250	0.63714	0.97032
Exc_L4_6_LRRK1	0.0179	0.87329	0.97032
Exc_L4_PLCH1	-1.3193	0.75646	0.97032
Exc_L5_6_PDZRN4	0.5294	0.14456	0.57822
Exc_L6_TLE4	0.2510	0.81081	0.97032
Exc_L6_TSHZ2	0.1982	0.82872	0.97032
Inh_CGE_LAMP5	-0.9975	0.45480	0.97032
Inh_CGE_MGE_CHST9	0.3834	0.47491	0.97032
Inh_CGE_NDNF	-0.0418	0.65974	0.97032
Inh_CGE_VIP	0.5493	0.08118	0.40589
Inh_MGE_B3GAT2	-1.4588	0.04519	0.40589
Inh_MGE_CALB1	-0.0065	0.97498	0.97805
Inh_MGE_PVALB	-0.0408	0.76213	0.97032
Inh_MGE_UNC5B	0.9846	0.22967	0.65621
NonN_Astro_FGF3R	0.1373	0.56920	0.97032
NonN_Micro_Endo_TYROBP	-0.0033	0.97805	0.97805
NonN_Oligo_MBP	-0.1277	0.07607	0.40589